FFI RAPPORT

BEAM SHAPING OF HIGH POWER LASER DIODE BARS

RUSTAD Gunnar, LIPPERT Espen, STENERSEN Knut

FFI/RAPPORT-2001/02647

FFIE/792/115

Approved
Kjeller 15 May 2001

Stian Løvold
Director of Research

BEAM SHAPING OF HIGH POWER LASER DIODE BARS

RUSTAD Gunnar, LIPPERT Espen, STENERSEN Knut

FFI/RAPPORT-2001/02647

FORSVARETS FORSKNINGSINSTITUTT
Norwegian Defence Research Establishment
P O Box 25, NO-2027 Kjeller, Norway

FORSVARETS FORSKNINGSINSTITUTT (FFI)
Norwegian Defence Research Establishment

P O BOX 25
N0-2027 KJELLER, NORWAY

UNCLASSIFIED

SECURITY CLASSIFICATION OF THIS PAGE
(when data entered)

REPORT DOCUMENTATION PAGE

1) PUBL/REPORT NUMBER	2) SECURITY CLASSIFICATION	3) NUMBER OF PAGES
FFI/RAPPORT-2001/02647	UNCLASSIFIED	41
1a) PROJECT REFERENCE	**2a) DECLASSIFICATION/DOWNGRADING SCHEDULE**	
FFIE/792/115	-	

4) TITLE

BEAM SHAPING OF HIGH POWER LASER DIODE BARS

5) NAMES OF AUTHOR(S) IN FULL (surname first)

RUSTAD Gunnar, LIPPERT Espen, STENERSEN Knut

6) DISTRIBUTION STATEMENT

Approved for public release. Distribution unlimited. (Offentlig tilgjengelig)

7) INDEXING TERMS

IN ENGLISH:	IN NORWEGIAN:
a) Semiconductor Laser Arrays	a) Halvlederlaserarrayer
b) Microlenses	b) Mikrolinser
c) Laser Beams	c) Laserstråler
d) Beam Steering	d) Strålestyring
e) Optical Focusing	e) Optisk fokusering

THESAURUS REFERENCE: **INSPEC 1999**

8) ABSTRACT

A technique for reshaping the highly astigmatic beam from a high-power laser diode bar by use of two parallel mirrors is studied theoretically and experimentally. It is found that the output from the 1 µm x 1 cm laser diode can be reshaped and focused down to a spot of <0.5 mm diameter with reasonably good beam symmetry +/- 5 mm from the focal plane. Experimentally, it was found that ~80% of the output power at the laser diode could be coupled into this spot. This is an efficient technique for laser-diode end-pumping of high-power solid-state lasers.

Further, several diode parameters that affect the design of the beam shaping system are investigated, and two main operating regimes are identified. For diodes with a small number (~20) of active regions, a geometry where the diode bar is imaged onto the mirrors should be used, whereas for diodes with a large number (~50) of active regions, a non-imaging geometry can be used. The imaging geometry offers better output beam quality, while the non-imaging geometry offers greater flexibility and easier alignment.

9) DATE	AUTHORIZED BY	POSITION
	This page only	
15 May 2001	Stian Løvold	Director of Research

ISBN-82-464-0513-6

UNCLASSIFIED

SECURITY CLASSIFICATION OF THIS PAGE
(when data entered)

CONTENTS

BEAM SHAPING OF HIGH POWER LASER DIODE BARS

1 INTRODUCTION

The need for efficient lasers with high average output powers is increasing. One important military application of such lasers is in countermeasures, in particular against heat seeking missiles and thermal imaging cameras applying the 3-5 µm wavelength band. To obtain the required output powers at such wavelengths in practical systems, non-linear conversion techniques are applied where the frequency of a high power pump source is shifted to the 3-5 µm band. The pump source in such systems is usually a diode-pumped solid-state laser, either a Neodymium-laser emitting at ~1 µm or a Thulium- or Holmium-laser emitting at ~2 µm. This report describes a technique which is used to couple the output from high-power diode laser arrays into such lasers to obtain efficient lasers with more than 10 W average output power.

The design of an effective laser requires that the pump light is effectively coupled into and absorbed in the laser material, and that the resulting gain distribution in the laser matches well with the laser mode distribution. One usually distinguishes between end-pumping and side-pumping geometries. In end-pumping geometries the pump light enters the laser crystal parallel with the laser mode, i.e. it enters the laser crystal at one or both ends. The advantage of this geometry is that good overlap between the pump and the laser mode usually can be obtained, giving potential for good beam quality and high efficiency. The disadvantage is that scaling of the output of the laser to the multi-watt regime is difficult because available high power laser diodes have a highly astigmatic emission, making focusing of the light through the (narrow) end faces of the laser rod and obtaining a good overlap with the resonator mode difficult. The side-pumping geometry in which the pump light enters the laser material transversally to the laser mode, can easily be scaled to higher pump power, but has disadvantages in terms of poorer overlap between the pump and laser mode distributions, leading to less efficient lasers. We have previously studied both these pump geometries for moderate pump powers [1-3]. In this work, we study a recently invented pump geometry [4] that allows higher pump powers to be obtained in an end-pumping geometry. This report concentrates on the pump geometry itself, whereas design of and results from laser experiments will be presented in later reports.

The light from commercially available laser diodes with output power above 20 W is usually highly astigmatic. They consist of a linear array of ~20 or more active regions which each consists of many small emitters. The resulting emitting area of the laser diode is typically 1 cm x 1 µm where the beam quality of the narrow dimension is M^2~1, whereas the beam quality in the wide direction may be $M^2 > 1000$. Several techniques of reshaping the output from such laser diodes have been proposed. These include coupling the light directly from individual active regions into optical fibers and collecting the 20-100 fibers into a bundle of ~1 mm diameter [5, 6], imaging the active regions onto an array of prisms, which ‘transposes’ the emission of the array and enables tighter focusing [7-9], as well as use of diffractive optical

components [10], arrays of microlenses [11-13], or by using tapered lens ducts [14]. All of these techniques suffer from transmission losses and, in most cases also of reduced brightness compared to the original diode emission. The technique we have found most promising was invented by Clarkson and Hanna at the University of Southampton [4]. In this geometry, the light from the different active regions are stacked on top of each other by use of two parallel mirrors. Transmission in excess of 90% and a far more symmetric beam can be obtained, giving potential for efficient multi-watt operation of end-pumped lasers. In some cases the brightness of the diode emission can also be increased by this technique.

This report describes the theory, design, and simulations of the beam transformation technique as well as experimental measurements of the transformed beam. A brief overview of the planned laser concept is given in Chapter 2 before presenting the laser diode pump sources in Chapter 3. The theory, design and simulations of the beam-shaper are described in Chapter 4, and measurements of the beam profile after the beam shaper are shown in Chapter 5.

2 LASER CONCEPT

A sketch of the planned laser set-up is shown in Figure 2.1. The pump source in this laser is a 20-50 W laser diode. The output from this diode is collected and imaged through a series of cylindrical lenses onto the beam shaper which consist of two parallel highly reflective mirrors placed at approximately 45 degrees to the incident beam. The reshaped output beam is focused through two crossed cylindrical lenses into the end of a laser rod. The laser will usually consist of two mirrors, the laser rod, and, perhaps, a Q-switch. To increase the laser output power further, the light from a second laser diode can be reshaped in a similar manner and focused into the laser rod through the other end. This report describes the diode laser, the beam-shaper, and the optics before and after the beam-shaper. Laser experiments with different laser materials will be described in separate reports.

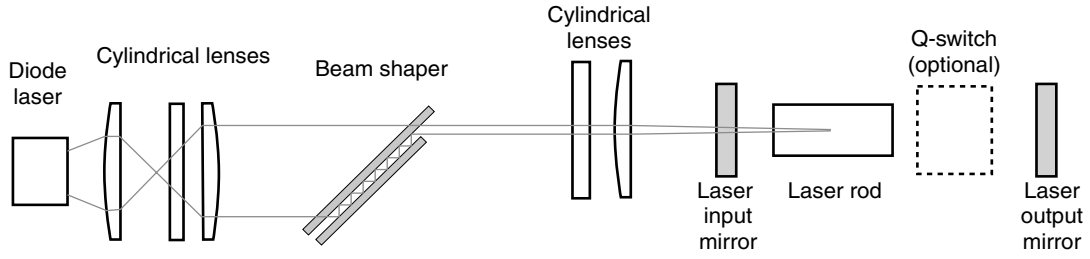

Figure 2.1 Schematic of the laser concept

3 THE DIODE LASER

We have bought high-power laser diodes from two different manufacturers (Coherent and IMC). These have much in common, but the geometries of the light emitting area of the diodes are different. As will be seen later, this has considerable influence on how the beam-shaper should be designed. All diodes will be briefly described in the following, but in most of the calculations for the beam shaper in Chapter 4, we have used the data for the diode from Coherent.

3.1 Diode laser geometry

The diode bars available to us are all 1 cm wide monolithic arrays consisting of a number of sub-arrays occupying 30-50 % of the total width of the bar, as illustrated in Figure 3.1a. A hyperbolic fiber lens (LIMO FAC850) mounted on the bar package is used to collimate the ~40° (FWHM) divergent output beam in the direction normal to the p-n junction (see Figure 3.1b). The resulting beam, even at wide emission angles, is well collimated, as can be seen in Figure 3.2 where results from ray-tracing calculations are shown. The beam profile in the collimated direction can be approximated by that of a Gaussian beam with 300-500 µm waist radius (40° FWHM divergence leads to 488 µm waist).

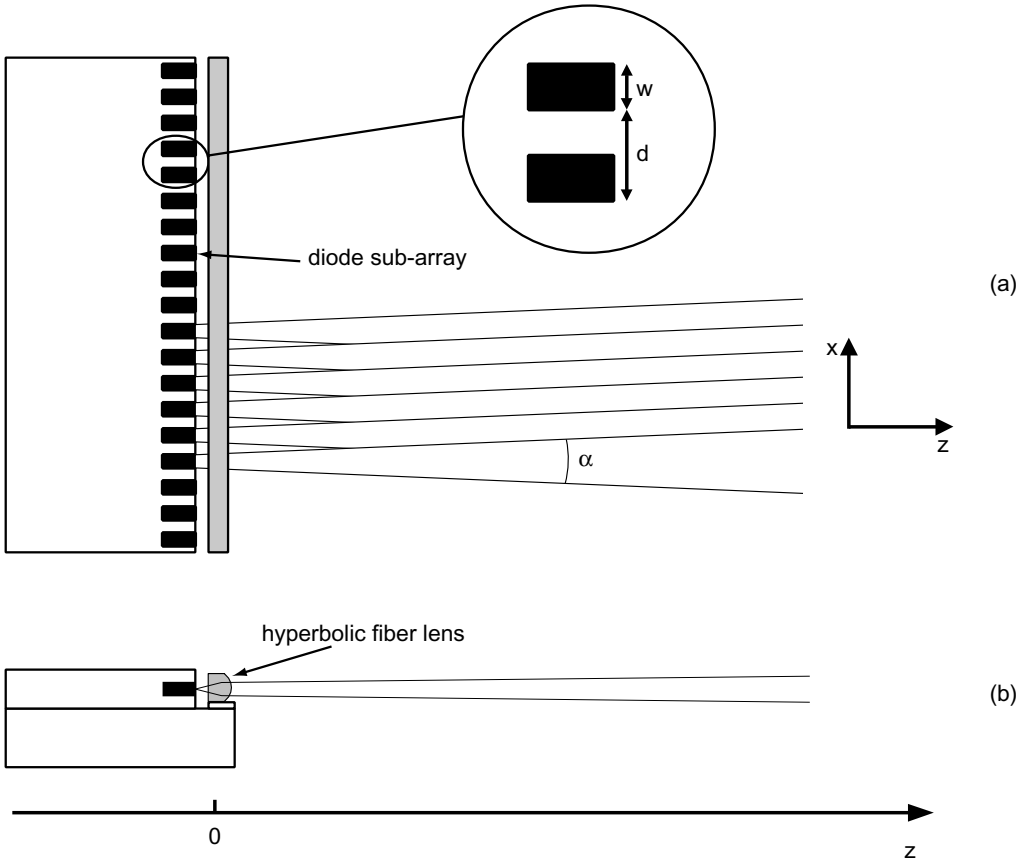

Figure 3.1 Diode bar layout seen from above (a) and from the side (b)

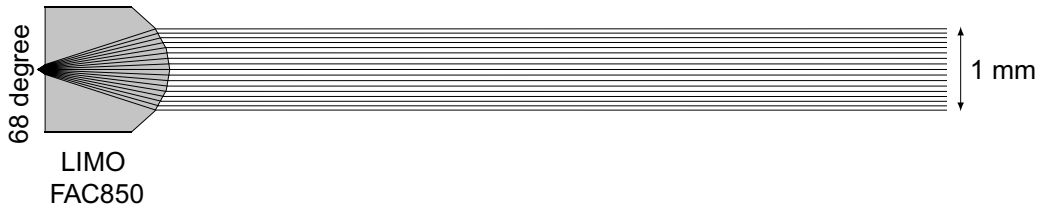

Figure 3.2 Ray-tracing calculation of the laser diode and the collimating lens. Good collimation is obtained up to a full angle of 68°

In the rest of this work, we will refer to the sub-arrays as **emitters**, and the beams from the emitters as a **sub-beams**. For later use we define the following coordinate system and general diode bar parameters:

x - direction parallel to the p-n junction

y - direction normal to the p-n junction

z - beam propagation direction

w - width of emitter (sub-array)

d - center-to-center spacing of emitters (sub-arrays)

N - number of emitters (sub-arrays)

α - beam divergence FW($1/e^2$)M parallel to the p-n junction for each emitter (sub-array)

ω_{01} - Gaussian beam waist radius normal to the p-n junction after collimation with the fiber lens

z_1 - position of beam waist of the collimated beam

λ - laser wavelength

P - nominal laser output power

BQ - beam quality: Product of beam diameter and beam divergence (FW($1/e^2$)M). At 780-800 nm wavelength, the value of this product in units of mm·mrad is approximately equal to the dimensionless M^2 beam quality factor

The main difference between the diodes from the two manufacturers is the geometry of the diode bar. While the diode from Coherent consists of 19 emitters, each 150 µm wide, the IMC diodes consist of 48 emitters, each 100 µm wide. In Table 3.1, the data for the diodes are summarized.

	w µm	**d** µm	**N**	α mrad	ω_{01} µm	z_1 mm	λ nm	**P** W	**BQ$_x$** mm·mrad
Coherent	150	500	19	50	300	-100	785	30	500
IMC	100	200	48	117	-*	-*	806	40	1170

*Table 3.1 Summary of laser diode parameters. *) The output from the IMC diodes was multi-transverse in the y-direction and it was not possible to deduce a value for ω_{01} and z_1*

There is no phase correlation between different emitters, so the total bar is essentially incoherent with a divergence equal to that of each emitter. In the y-direction, the beam quality is approximately that of a Gaussian beam, i.e. M^2~1 or about 1 mm·mrad for ~800 nm wavelength.

For the diode from Coherent, the divergence in the y-direction after the collimating lens was about 1.7 mrad given by

$$\alpha_y = \frac{2\lambda}{\pi\omega_{01}} \ . \tag{3.1}$$

3.2 Transverse modes in the y-direction

It has commonly been assumed that the field in the y-direction from a laser diode consists of the fundamental Gaussian mode. However, we have observed that this is not the case for our diodes. In the far field of the collimated diodes, it was observed for all diodes that there were two or more ‘lobes’ in the collimated direction. These lobes had slightly different direction of propagation and divergence angles. For the Coherent diode, the pattern consisted of a strong main lobe, and a weaker side lobe, while for the IMC diodes, the pattern was more complicated and consisted of several lobes. In Figure 3.3, a photograph of the main mode and side mode is shown for the Coherent diode.

Neither diode manufacturer was aware of this mode pattern, nor could they provide an explanation of its origin. We believe that these modes stem from different eigenmodes of the waveguide structure in the laser diode. The multi-mode structure is undesirable as it may be difficult to couple all light through the input aperture of the beam shaper. This may therefore reduce the useful pump power from the laser diode.

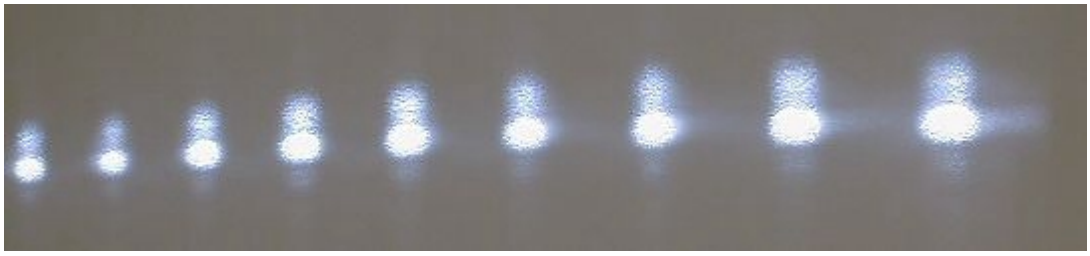

Figure 3.3 Photograph of the main and the side mode in the far field of the Coherent diode. The image of the laser diode was magnified in the x-direction by a 25 mm cylindrical lens

3.3 Smile-effect

Ideally, the emitters should be positioned along a straight line in the x-direction. There is, however, often a variation of a few microns in the vertical (y-) positions of the emitters along the array. This is commonly called the smile-effect, which after collimation with the fiber lens results in a variation in the vertical pointing direction of the beams from the emitters. As shall be seen in the next chapter, the smile-effect may have a detrimental effect on the transmission through the beam-shaper.

The smile for each diode was found by measuring the height and shape of the emission from each emitter by a knife-edge scan. This was done behind a 25 mm cylindrical lens in the x-direction which magnified the image of the diode bar enough that the individual emitters could be characterized (see Figure 3.3). The results of these measurements are shown in Figure 3.4. In the calculations in the next chapter where the smile-effect has been accounted for, we have used the measured smile-effect of the Coherent laser diode.

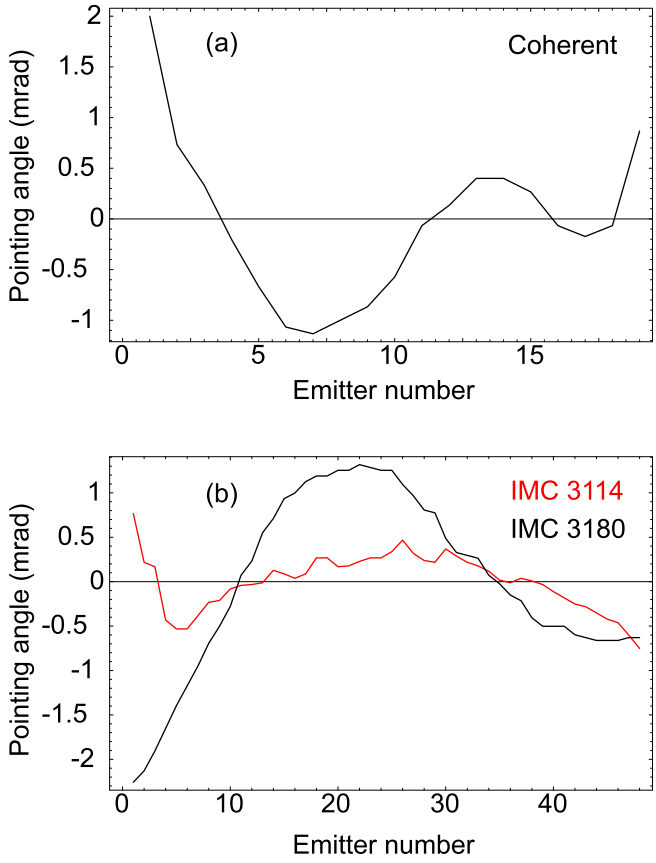

Figure 3.4 The measured smile-effect of the laser diodes from (a) Coherent and (b) IMC

4 THE BEAM TRANSFORMATION METHOD

4.1 Principle and theory

4.1.1 The beam shaper

The main objective of the beam transformation is to reduce the high aspect ratio of the output beam from the diode array and provide a reasonably symmetric pump beam in the diode pumped laser rod. The main principle of the method used here is to provide a transformation such that the output beams from the N emitters are stacked on top of each other instead of side-by-side, as illustrated in Figure 4.1.

The transformation is performed in the following way: L1 and L3 provide an image of the diode array at the beam shaper BS, with a magnification $M \approx f_3/f_1$ in the x-direction. L2 provides a refocusing of the beam in the y-direction, such that the beam acquires a new vertical beam waist with radius ω_{02} at the center of the BS (i.e. the z-position where the center sub-beam from the diode bar hits the BS). The BS consists of two parallel, highly reflective mirrors with separation s. The mirrors are placed at an orientation that is described by the angles θ and ϕ, where θ is the angle between the surface normal of the mirrors and the x-z-plane (typically 10-12°), and ϕ is the angle between the x-axis and the intersection of the mirrors in the x-z-plane (typically 45°). The top edge (TE) of the first mirror of the BS is positioned such that the

beams from the diode bar pass just above it with minimal clipping. The sub-beams are reflected by the second mirror, and, because the mirrors are tilted, the reflected beams will experience multiple reflections between the mirrors, until they escape past the vertical edge (VE) of the second mirror, as indicated in Figure 4.1. The mirrors have HR coatings that cover the mirror surfaces all the way to the critical edges, TE and VE. At the output of the BS the images of the sub-beams from the emitters are stacked on top of each other. Each beam has a width of $M \cdot w$ in the x-direction and a beam radius ω_{02} in the y-direction, which will be discussed in more detail in connection with Figure 4.13.

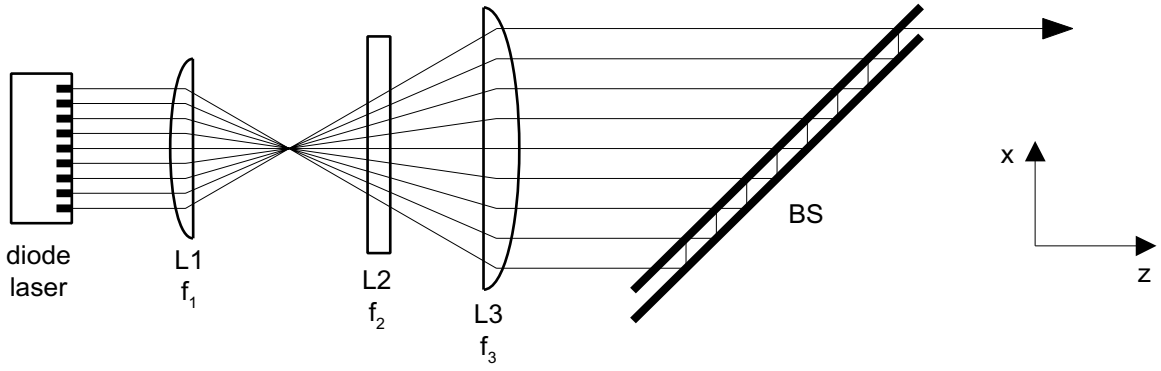

Figure 4.1 Top view of beam transformation technique. L1-L3: Cylindrical lenses with focal lengths $f_1 - f_3$ BS: Beam shaper, consisting of 2 parallel mirrors

In order for the sub-beams to be exactly on top of each other at the exit aperture, the x-displacement Δ_x in each reflection must be equal to the center-to-center distance of the emitters in the magnified image, i.e. $\Delta_x = M \cdot d$. For diode bars with a large number ($\gtrsim$30) of emitters one may wish to stack 2 or more sub-beams side by side at the output from the BS to reduce the height of the output beam. In such cases the x-displacement should be $\Delta_x = k \cdot M \cdot d$, where k is the number of sub-beams stacked in each row. However, as will be seen in Section 4.1.3, choosing $k > 1$ will lead to clipping of some of the sub-beams at the exit aperture. We will therefore assume $k = 1$ in the following and return to the case of $k > 1$ in Section 4.2.3.2.

The y-displacement Δ_y in each reflection should be as small as possible in order to have a narrow stacked beam in the y-direction at the output of BS. However, since Δ_y also represents the vertical entrance aperture of the BS as seen by the beams, it must be large enough to avoid significant clipping and loss of power.

The horizontal and vertical displacements per (double) reflection in the BS can be expressed in terms of the mirror spacing s and the angles θ and ϕ defined above:

$$\begin{aligned} \Delta_x &= 2s\cos\theta\sin\phi \\ \Delta_y &= 2s\sin\theta \end{aligned} \quad . \tag{4.1}$$

s, θ and ϕ are selected in order to satisfy $\Delta_x = M \cdot d$ and to obtain a suitable value of Δ_y. The optimal value for Δ_y depends on the vertical beam radius ω_{02} and the magnitude of the smile-effect and transversal mode pattern discussed in Sections 3.2 and 3.3. This will be discussed in more detail in Section 4.1.2 below.

Using (4.1) and requiring that $\Delta_x = M \cdot d$, we obtain the following relation which will be used later in the report:

$$\Delta_y = M \cdot d \frac{\tan\theta}{\sin\phi}. \tag{4.2}$$

In order for the sub-beams to be stacked on top of each other, we also have to adjust VE of the second mirror in the BS such that the projection of VE in the x-y plane is vertical. This can be achieved by rotating the second mirror an angle γ about an axis normal to the mirror. If VE was vertical before the mirror was rotated ϕ and θ, i.e. for $\phi = \theta = 0$, the required rotation angle γ is given by:

$$\gamma = \arctan\left(\sin\theta \tan\phi\right). \tag{4.3}$$

It should be observed that the adjustment of γ does not affect Δ_x or Δ_y, so this adjustment can be made after the other parameters (s, θ, ϕ) have been set. In addition, VE must be translated in the x-direction in order for the stacked beams to be centered in the BS output aperture, defined by VE and the horizontal displacement Δ_x.

Finally, in order to maximize the transmittance through the BS, the top edge TE of the first mirror in the BS must be adjusted such that its projection onto the x-y plane is parallel to the magnified image of the diode array (i.e. approximately horizontal), and such that the image is centered in the BS input aperture, defined by TE and the vertical displacement Δ_y. This is achieved by a rotation about the mirror normal and by a vertical translation.

From (4.1) we observe that Δ_x is almost independent of θ for relevant values of θ (<5% reduction of Δ_x for $\theta = 0 \rightarrow 18^\circ$). Consequently, θ can be used to adjust Δ_y without affecting Δ_x significantly. In order to obtain the desired values of Δ_x and Δ_y we have found the following procedure to be convenient: First, we set ϕ to about 45° and θ to ~12°, and adjust s in order to obtain the desired Δ_x. Then θ is adjusted to obtain the desired Δ_y, and, if necessary, a final fine adjustment of s or ϕ can be made in order to optimize Δ_x and obtain exact vertical stacking of the beams at the output of the BS. A more detailed discussion concerning alignment procedures for the entire beam transformer system is given in Section 4.2.

Typical parameter values used in the experiments described in this report are: d = 0.5 mm, M = 2, s = 0.72 mm, ϕ = 45°, and θ = 12°, which gives Δ_x = 1 mm (=$M \cdot d$), and Δ_y = 0.3 mm. The choice of Δ_y is related to the transmission through the beam shaper and will be discussed below.

In general, when choosing parameter values, considerations must be made regarding the input and output apertures, the difference in path length through the BS for the different sub-beams, mirror sizes, imperfections in the laser diode (smile, higher order transversal modes), and requirements concerning the symmetry of the pump beam after it is focused into the laser rod. These aspects will be discussed in some detail later.

4.1.2 Transmission through the beam shaper

As discussed above, the input aperture is defined by the top edge (TE) of the first mirror and Δ_y. However, in calculating the transmission through the input aperture, one must also account for the fact that the different sub-beams hit the BS at different z-positions relative to their beam waists. In Figure 4.2, the transmission is shown as function of the input aperture size assuming a 20 mm wide magnified array of sub-beams at the BS, a 50 µm vertical beam waist ω_{02} at the center of the BS, and ϕ = 45º. We observe that good transmission can be obtained with input apertures as small as 200 µm for diodes without the smile-effect. However, as was shown in Figure 3.4, this is not always the case. Also shown in Figure 4.2 is the calculated transmission when the measured smile-effect for the Coherent laser diode in Figure 3.4(a) was taken into account and the lens system between the laser diode and the BS was adjusted to minimize the smile-effect at the position of the BS (see Section 0 for details about this).

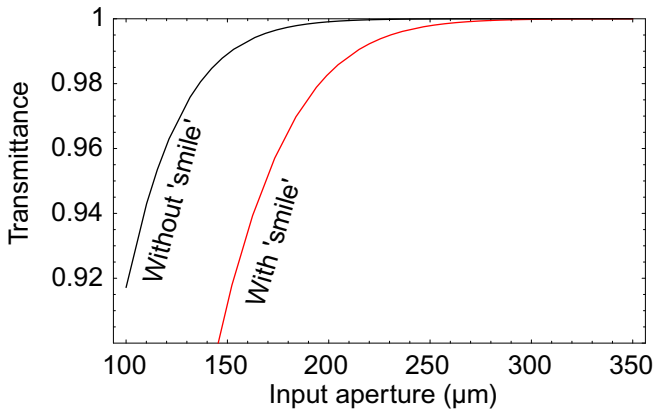

Figure 4.2 *Transmittance through the BS input aperture as a function of aperture height for an input beam waist radius of 50 µm at the center of the BS, 20 mm beam width at the BS, and ϕ=45º. Also shown is the transmission when the smile-effect in Figure 3.4(a) is accounted for*

For a given input aperture it is clear that the transmission will be higher for smaller ϕ since each sub-beam can be closer to its waist when it hits the BS. On the other hand, it is also clear that the difference in path length at the exit aperture for the different sub-beams will increase as the angle ϕ is reduced. The difference in path length between adjacent sub-beams is given by:

$$\Delta L = \left(\frac{2}{\cos\theta \sin 2\phi} - \tan\phi \right) M \cdot d \,, \tag{4.4}$$

A larger ΔL will lead to a reduced beam quality of the output beam from the BS because the spread in propagation distance between the individual emitters is greater. Figure 4.3 shows how the transmission is increased and how the difference in path length is increased at smaller ϕ.

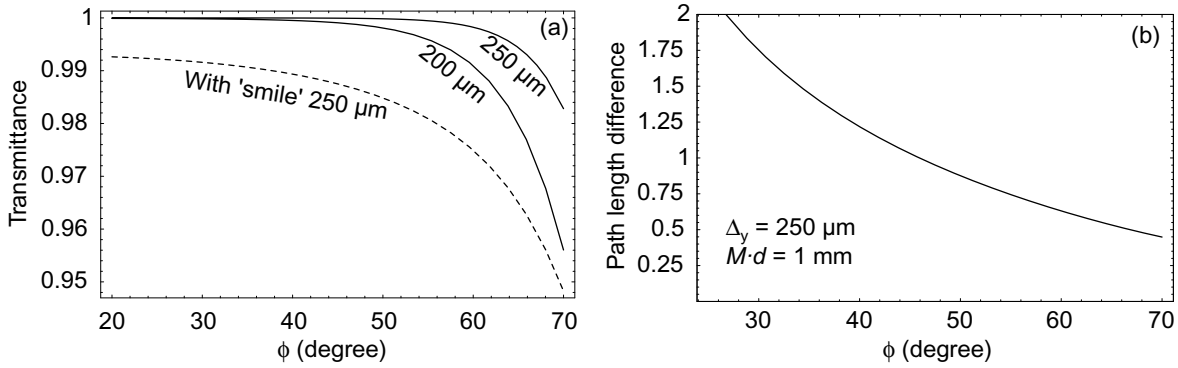

Figure 4.3 *(a) Calculated transmission through 200 µm and 250 µm apertures as function of the angle ϕ for diodes without smile and through a 250 µm aperture accounting for the smile-effect shown in Figure 3.4(a). ω_{02} = 50 µm in all cases. (b) Calculated difference in path length for adjacent sub-beams relative to the distance between the sub-beams. Here, θ and s was adjusted as ϕ was varied to keep $\Delta_y \equiv$ 250 µm and $\Delta_x \equiv$ 1 mm*

Finally, the required size of the mirror also increases with increasing ϕ:

$$W_{mirror} = \frac{N \cdot M \cdot d}{\cos\phi} \quad , \tag{4.5}$$

where N is the total number of sub-beams, i.e. $N{\cdot}M{\cdot}d$ is the total width of the beam at the BS.

In this work ϕ has been chosen to be 45° as a compromise between the different requirements. The choice of θ directly relates to the input aperture according to (4.2). With M = 2, d = 0.5 mm, and ϕ = 45°, we find that $\theta \approx 12°$ gives 300 µm input aperture, which was seen to be the smallest practical aperture for the current laser diode.

The transmission through the BS is also affected by the mirror reflectance. If we number the sub-beams, starting with 1 at the beam that passes the BS without reflection, then sub-beam number m has been reflected 2(m-1) times. If R is the reflectance of the mirrors, then the transmittance through the mirror system is given by

$$T = \frac{1}{N}\sum_{m=0}^{N-1} R^{2m} = \frac{1-R^{2N}}{N\cdot\left(1-R^2\right)} \quad . \tag{4.6}$$

The transmission for N = 19 is shown in Figure 4.4 as function of R. It is clear that, owing to the high total number of reflections, N (N-1), the transmission is vulnerable to even small losses in the BS mirrors. The total transmission of the beam shaper is found from the combination of this transmission and the transmission through the entrance aperture in Figure 4.3.

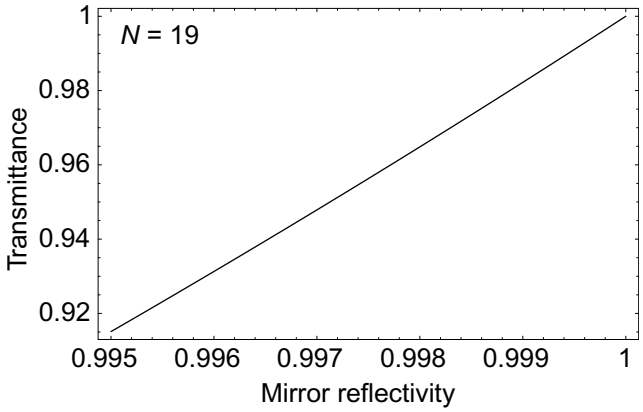

Figure 4.4 Calculated transmittance through the BS mirror system as function of mirror reflectivity

4.1.3 The lens system before the beam shaper

The purpose of the optics between the laser diode and the BS is to image the diode-bar with a certain magnification in the x-direction at the position of the BS, and to focus the beam to a suitable diameter at the BS in the y-direction. The advantages of a magnification in the x-direction is partly that the exit aperture of the BS is bigger, making it easier to align, and partly that the divergence in the x-direction after the BS is reduced. The disadvantage is that larger mirrors (and larger lenses) are needed and that the transmission in the BS is reduced because the difference in path length is bigger and may become comparable to the Rayleigh length in the y-direction. In this work we have chosen to use a magnification of ~2 which seems to be a reasonable choice.

In the y-direction, the beam should be focused to a beam waist radius of 30-80 µm for optimum transmission through the BS, as can be seen in Figure 4.5. A too large focus will obviously lead to aperture losses, but also a too small focus will lead to this since the Rayleigh length will be short compared to the path difference between center and side beams, leading to a clipping of the side beams.

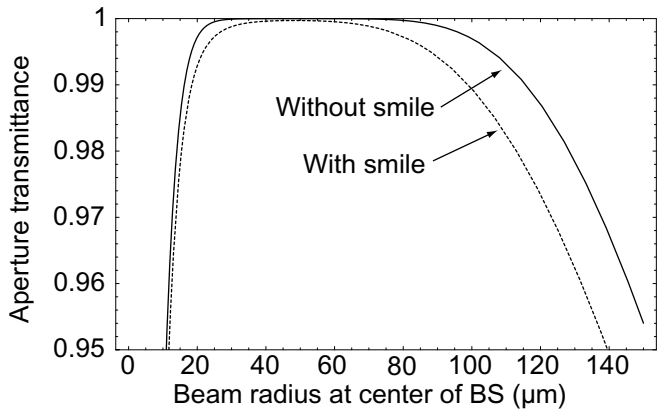

Figure 4.5 Calculated transmittance through a 300 µm BS input aperture as function of beam waist radius at the center of the beam shaper for beams with and without the smile-effect. A 20 mm total width at the BS was assumed

Additionally, the size of the focus at the beam shaper also influences on the size of the focus that can be obtained after the BS (i.e. inside the laser rod). In Figure 4.18 in the next section,

the shape (in the y-direction) of the beam in the focal plane of a 40 mm cylindrical lens placed 150 mm after the beam shaper is shown for 25 µm and 50 µm beam radii at the beam shaper. It is clear that a larger focus at the BS leads to a smaller focus in the laser rod. One might argue that a more narrow focus could be obtained by a stronger lens. This will, however, also affect the divergence of the beam and thereby the 'volume' of the focused beam inside the laser rod. Therefore, the beam size at the BS should be chosen as large as possible, i.e. 60-70 µm radius in this case or even larger if some aperture loss can be accepted.

If the beam has a Gaussian profile in the y-direction with a waist radius ω_{01} after collimation at the output of the laser diode, and is focused by a lens of focal length f placed a distance a from the waist position, the beam will be focused to a new waist radius ω_{02} at a distance b from the lens according to the relations:

$$z_{02} = \frac{f^2}{(a-f)^2 + z_{01}^2} z_{01}$$

$$b = f + \frac{z_{02}}{z_{01}}(a-f) \qquad (4.7)$$

$$z_{0i} = \frac{\pi \omega_{0i}^2}{\lambda}$$

Here, b is the distance from the lens to the new waist and we recognize z_{0i} as the respective Rayleigh lengths. By inserting ω_{01}=300 µm and assuming $a + b$ = 250 mm (i.e. the distance between the laser diode and the BS plus the value of z_1 in Table 3.1), we find that a 60 mm lens gives 50 µm waist radius, and a 100 mm lens gives 80 µm waist radius. For such configurations we find that b deviates from f by less than 1 mm.

To obtain a reasonably compact and simple lens system for the imaging in the x-direction, a system of two cylindrical lenses was chosen. Since the beam is very wide (1 cm at the diode and 2 cm after magnification) this results in the use of low f-number lenses and thereby aberrations. In Figure 4.6 a plot of the ray-tracing of the center beam, a beam 2.5 mm from center, and the edge-beam 5 mm from the center is shown. The lenses chosen were f = 25.4 mm and f = 50 mm cylindrical lenses from Melles Griot. The distance between these lenses were chosen to be 66 mm to ensure that the sub-beams are parallel after L3.

The position of the two-lens system relative to the laser diode will affect the position of the image of the laser diode behind L3. The closer the lens system is to the diode, the further away from L3 is the image of the laser diode. The exit aperture of the BS is typically placed 50 mm behind L3. In Figure 4.7, the sizes of the three different sub-beams at this position are shown as function of distance between the laser diode and L1 (with the L1-L3 distance fixed at 66 mm). These simulations were performed assuming that the 150 µm wide emitters have a 50 mrad top-hat divergence.

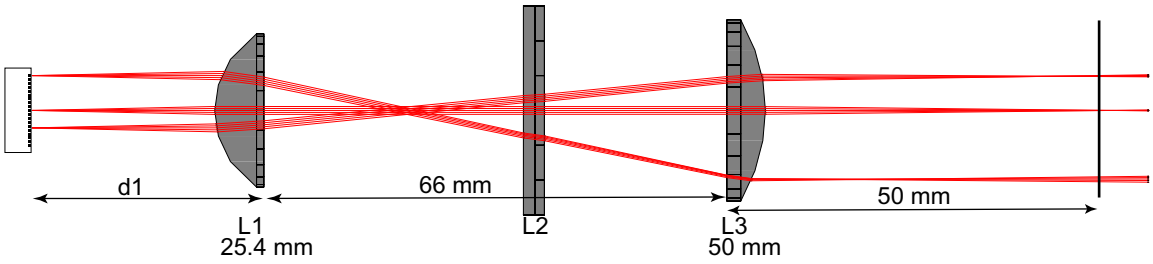

Figure 4.6 *Ray-tracing of three emitters through the lens system. The vertical line to the right indicate the position of the exit aperture of the BS*

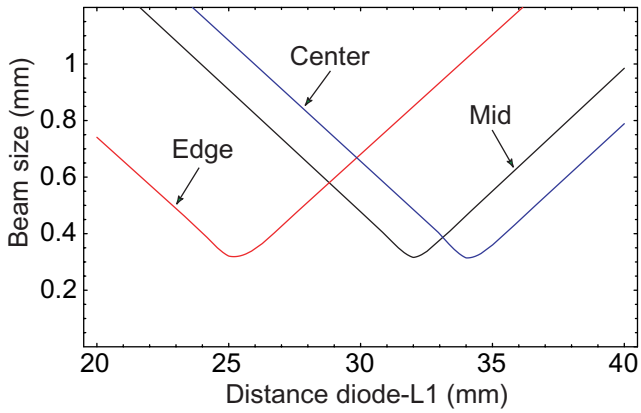

Figure 4.7 *Calculated beam size in the x-direction 50 mm after L3 as function of distance between the laser diode and L1. The 150 µm wide emitters were imaged by the lens system in Figure 4.6 (M ≈ 2) assuming a 50 mrad full width top-hat divergence*

In Figure 4.8, the calculated beam sizes for the center, mid and edge sub-beams are shown as function of distance from L3 with a fixed lens system at *d1*= 28 mm and L1-L3 = 66 mm. We can clearly see the aberrations of the lens system since the sub-beams have their minimal beam sizes at different positions.

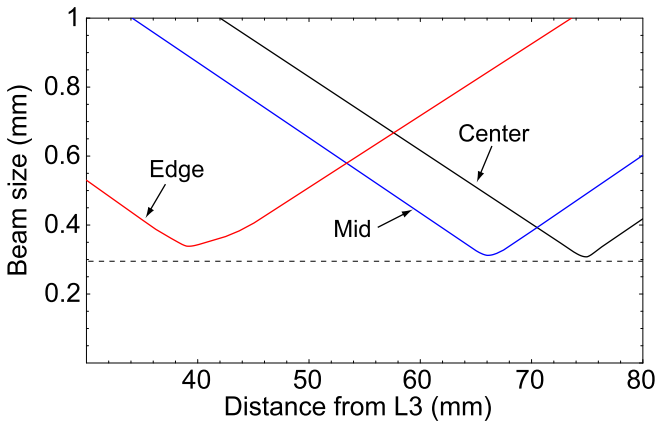

Figure 4.8 *Calculated beam size in the x-direction as function of distance from L3 for the center sub-beam, a sub-beam 2.5 mm from the center (mid), and a sub-beam 5 mm from the center of the diode bar (edge). The 150 µm wide emitters were imaged by the lens system in Figure 4.6 (M ≈ 2) assuming a 50 mrad full width top-hat divergence. The dashed line indicates the minimum obtainable beam size (300 µm)*

The difference in propagation length for the different sub-beams at the exit aperture of the BS should also be regarded. In Figure 4.9, ray-tracing calculations similar to those in Figure 4.8 have been combined with the calculated difference in path length through the BS according to (4.4) to find the position of the minimum beam size for each sub-beam *relative to the exit aperture of the BS*. We observe that there is a considerable difference in the location of these minima across the diode bar. In the calculations, *d1* = 28 mm, L1-L3 = 66 mm, L3-BS exit = 50 mm, $\theta = 12^{\circ}$, and $\phi = 45^{\circ}$.

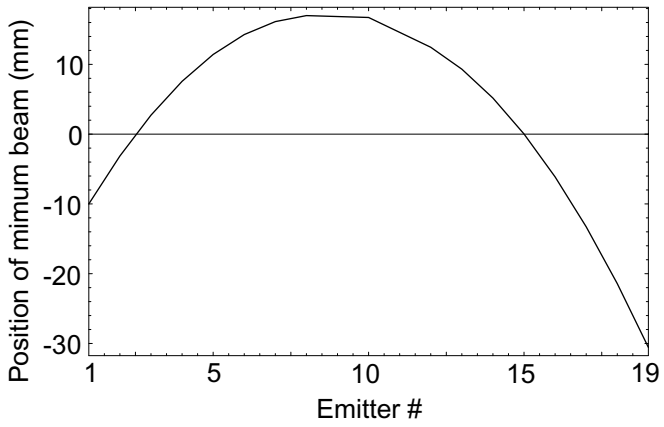

Figure 4.9 Calculated position of minimum beam size relative to the exit aperture of the BS accounting for aberrations in the lens system and path length differences in the BS

It is clear that this difference in position for minimum beam size will lead to a difference in beam size for the different sub-beams at the exit aperture of the BS. The differences in propagation distance are taken into account in Figure 4.10, which shows the calculated beam size at the exit aperture for different sub-beams for different values of *d1*. The simulations were performed using ray-tracing calculations through the system in Figure 4.6 assuming 150 µm wide emitters with a 50 mrad full width top-hat divergence. It is important that the sizes of the sub-beams at the exit aperture are smaller than the exit aperture to avoid clipping of the sub-beams. We note that by a proper choice of *d1*, this can be achieved for the simulated system. For diode bars with a higher number of emitters, like the IMC bars with 48 emitters, it is clear that stacking of e.g. two sub-beams side by side will lead to clipping at the exit aperture; in this case the exit aperture will still be approximately 1 mm, while the minimum beam size is increased from 300 µm to 600 µm ($M \cdot (d + w)$), and the divergence angle is significantly larger. The consequence of a larger beam divergence is that the beam is larger at positions off its minimum value. We propose a 'non-imaging' geometry for such diode bars in Section 4.2.3.2.

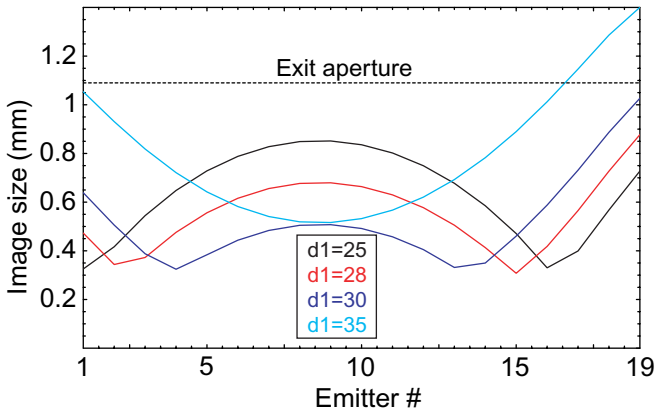

Figure 4.10 Calculated beam size at the exit aperture in a BS with ϕ =45º and θ=12º where the difference in path-length in the BS is accounted for. The calculated size is shown for 4 different diode-L1 distances, d1

4.1.3.1 Reduction of smile

The smile-effect describes the fact that the individual emitters may have slightly different pointing angles, and thereby, slightly different vertical positions at the position of the BS. It is possible to compensate partly for this effect by tilting the cylindrical lens L1 a few degrees in the yz-plane. This is based on the fact that the thickness of the lens observed by a beam near the edge of the lens is smaller than for a beam near the center of the lens. When the lens is tilted, this leads to a different shift in vertical (i.e. y-) position which also resembles a kind of smile across the beam. At an optimum angle the spread in vertical positions at the BS will be minimal, giving maximum transmission through the input aperture. In Figure 4.11, the calculated transmission of the Coherent diode based on ray-tracing calculations is shown for 250 µm and 300 µm apertures and 50 µm beam radius at the beam shaper as function of angular tilt of L1. In the ray-tracing calculations, the focal lengths of L1, L2, and L3 were 25 mm, 60 mm and 50 mm, respectively. For the transmission curve with smile-effect in Figure 4.2, the optimum value of 5° was assumed. Taking the smile-effect as well as alignment tolerances into account, we conclude that the minimum practical aperture in our experimental setup is limited to about 300 µm. In Figure 4.12 the calculated vertical positions of the different emitters at the BS are shown without and with a 5 degree lens tilt. It is clear that the maximum deviation from the straight line is reduced with the lens tilt.

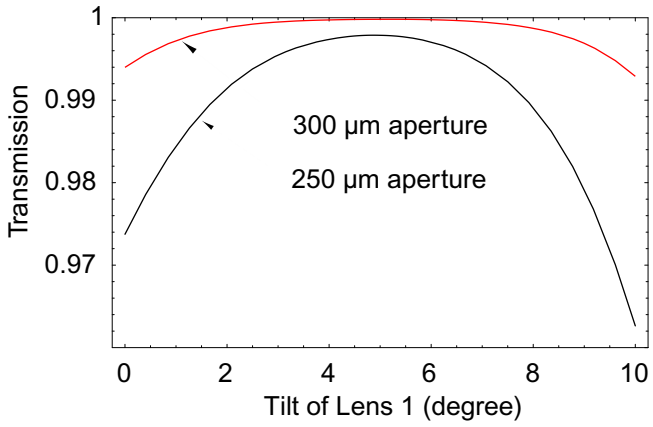

Figure 4.11 Transmittance through the BS input aperture as a function of angular tilt of L1 for 50 µm beam waist radius and 250 µm and 300 µm input apertures

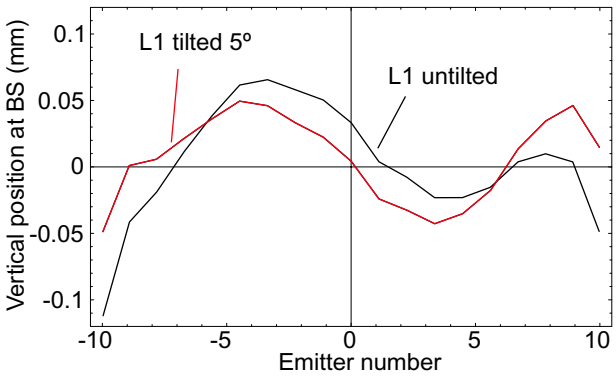

Figure 4.12 Calculated vertical position at the BS with untilted L1 and with L1 tilted 5º

4.1.4 The lens system after the beam shaper

The beam pattern at the output of the BS is sketched in the left part of Figure 4.13. The dimensions of each sub-beam will be approximately $M \cdot w$ = 300 µm in the x-direction for w = 150 µm and M = 2, and 100 µm (FW($1/e^2$)M) in the y-direction for ω_{02} = 50 µm. As discussed in Section 4.1.3, there is a variation in these dimensions due to the fact that the sub-beams have propagated different distances through the BS and also from the aberrations in the imaging system. As was seen in Figure 4.9, the positions of the smallest beam size of the different sub-beams vary with 47 mm in z-direction in the output beam from the BS. As the sub-beams propagate away from the BS, they diverge and overlap each other in the y-direction, as illustrated in the right part of Figure 4.13. The divergence in the x-direction will be α/M, where α is the divergence at the output from the diode bar. The divergence in the y-direction will be that of a Gaussian beam with a beam waist radius of ω_{02}, i.e. $2\lambda/(\pi\omega_{02})$.

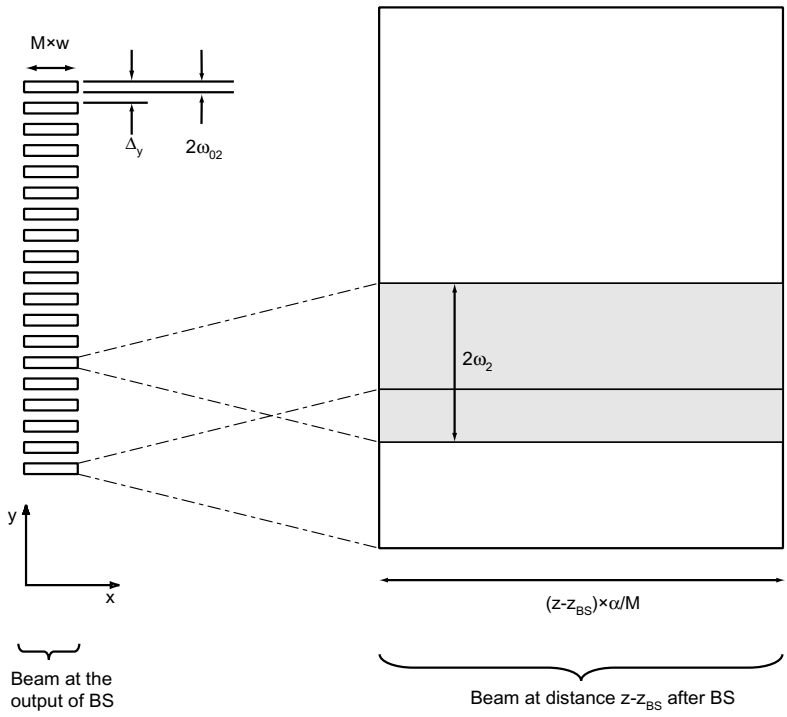

Figure 4.13 Beam pattern at the output of the BS (left) and at a distance z-z_{BS} after the BS (right)

The final step in the beam transformation is focusing of the beam after the BS. This is performed by two cylindrical lenses L4 (x-direction) and L5 (y-direction), as shown in Figure 4.14.

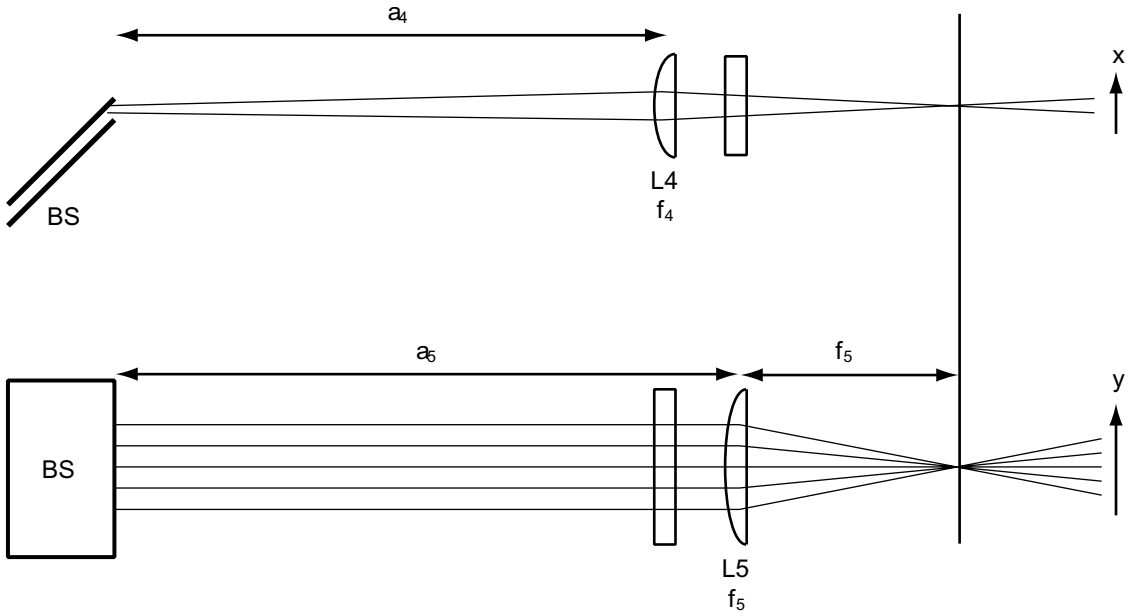

Figure 4.14 Final focusing of the output from the BS in the x-direction (upper part) and y-direction (lower part, only 5 of the sub-beams are indicated). L4 and L5 are cylindrical lenses.

4.1.4.1 Focusing in the x-direction

We have seen that the image of each emitter in the vicinity of the output from the BS has a width $M \cdot w$, where w is the width of each diode emitter and M is the x-magnification between the diode bar and the BS. With the parameters defined in Figure 4.14, the image width w_x after focusing with L4 becomes

$$w_x = \frac{f_4}{a_4 - f_4} M \cdot w \ , \tag{4.8}$$

and the distance from L4 to this image is given by

$$b_4 = \frac{a_4 f_4}{a_4 - f_4} \ . \tag{4.9}$$

The far field divergence α_x of this image becomes

$$\alpha_x = \frac{w}{w_x} \alpha = \frac{a_4 - f_4}{M \cdot f_4} \alpha \ , \tag{4.10}$$

and the beam quality is

$$BQ_x = w_x \alpha_x = w \cdot \alpha \ . \tag{4.11}$$

As expected, the beam quality for a single sub-beam is independent of M, a_4, and f_4, and is equal to the beam quality of the sub-beam at the output of the diode bar. Assuming w = 150 µm, α = 50 mrad, M = 2, f_4 = 50 mm, and a_4 = 150 mm, we find that w_x = 150 µm, b_4 = 75 mm, α_x = 50 mrad, and BQ_x = 7.5 mm·mrad. If the lens system between the diode and the BS imaged all sub-beams onto the exit aperture, then this would also have been the characteristics for the total beam in the x-direction.

Unfortunately, this is not the case, as was seen in Figure 4.9. The difference in position of the minimum beam size will both affect the sizes and positions of the images of the sub-beams after L4, as well as the far field divergence angle, since the distance a_4 will be different in (4.8), (4.9), and (4.10). In Figure 4.15 the image size, z-positions of the image, and divergence of each sub-beam behind L4 are shown for the case of *d1*=28 mm in Figure 4.10.

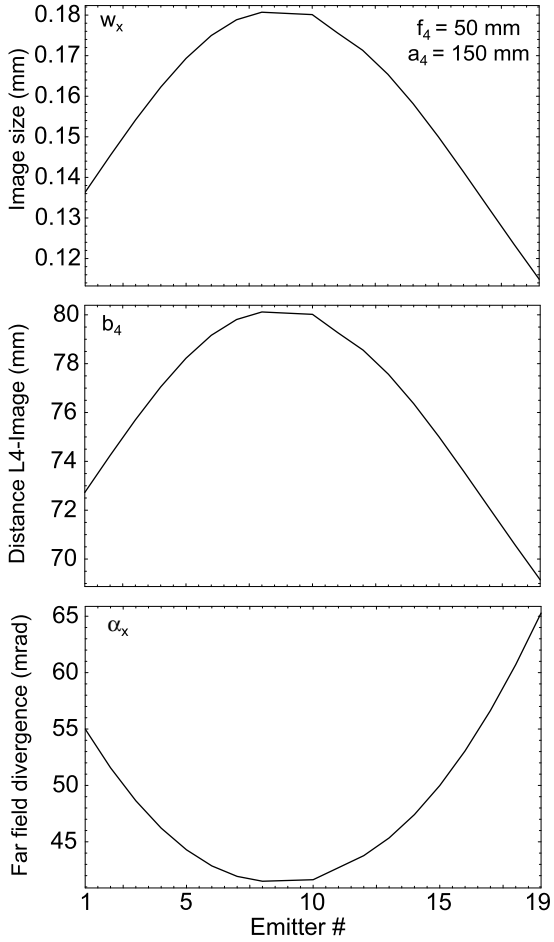

Figure 4.15 Calculated image size, position of image, and far field divergence of each sub-beam after a 50 mm lens 150 mm from the BS.

This will influence on the size and shape of the focus behind L4. In Figure 4.16, the total beam width is plotted as function of distance from L4. The beam diameter was estimated by adding 19 top-hat beams with equal power using the focusing parameters shown in Figure 4.15, and smoothing the total beam by a stepwise linear function. The diameter was found at the $1/e^2$-level of this function. We observe that the beam diameter at the focus is ~350 µm, i.e. more than twice that of each emitter. The beam quality of this beam was 20 mm·mrad.

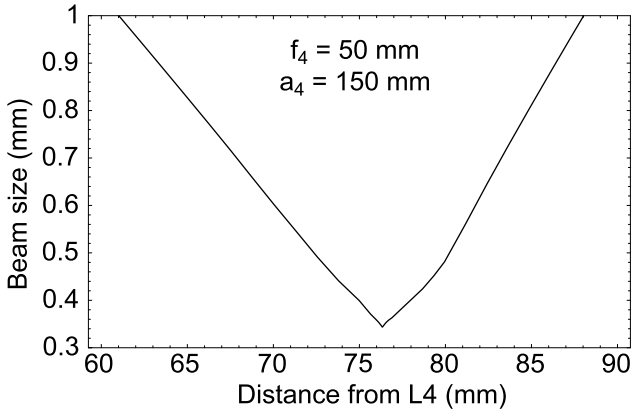

Figure 4.16 Calculated beam diameter in the x-direction after a 50 mm lens placed 150 mm behind the BS using the sub-beam parameters from Figure 4.15

4.1.4.2 Focusing in the y-direction

As discussed before, the beams from the different emitters are stacked on top of each other at the output of the BS, with a center-to-center separation Δ_y given by Equation (4.1). Each sub-beam is assumed to have a beam waist radius of ω_{02} at the center of the BS. The sub-beams after the BS are parallel to each other and will therefore cross each other in the focal plane of the lens L5. The beam radius in the focal plane is equal to the far field divergence of the incoming sub-beams multiplied by the focal length f_5 of L5. The beam diameter w_y in the focal plane therefore becomes:

$$w_y = 2\frac{\lambda}{\pi\omega_{02}} f_5 \quad . \tag{4.12}$$

The far field divergence α_y of this image is approximately equal to the total beam height after the BS divided by the focal length f_5, i.e.:

$$\alpha_y \approx \frac{N \cdot \Delta_y}{f_5} \quad . \tag{4.13}$$

The beam quality becomes

$$BQ_y = w_y \alpha_y = \frac{2N\lambda}{\pi}\frac{\Delta_y}{\omega_{02}} \quad . \tag{4.14}$$

Assuming ω_{02} = 50 µm, Δ_y = 300 µm, f_5 = 25 mm, N = 19, and λ = 0.79 µm, we find that $w_y \approx$ 250 µm, $\alpha_y \approx$ 230 mrad, and $BQ_y \approx$ 58 mm·mrad. We observe that for the given assumptions $w_y \approx 0.7 w_x$, $\alpha_y \approx 4\alpha_x$, and $BQ_y \approx 3BQ_x$, i.e. the beam is quite asymmetric in the focal region. From Equation (4.14) we see that BQ_y is proportional to Δ_y/ω_{02} , which is 6 with the given assumptions. As can be seen in Figure 4.2, there is, in theory, potential for reducing the ratio Δ_y/ω_{02} somewhat without significant clipping by the BS input aperture. However, the mentioned problem with the smile-effect has prevented us from achieving this in the experiments.

In Figure 4.17, the calculated beam diameter after a 25 mm focusing lens placed 150 mm behind the BS is shown as function of distance from the lens. The beam was taken to have a 50 µm waist radius at the BS (ω_{02}). In contrast to the results in the x-direction, but as expected according to (4.12), the ~20 mm difference in path length through the BS did not have any effect on the size of the focus. Also shown is the calculated beam profile (in the y-direction) at three different positions around the focal plane. We see that the beam is focused to a spot of ~200 µm 10-90 diameter[1] (corresponds to w_y ~ 250 µm) while the image of the individual emitters appear at a greater distance from the lens (approximately 30 mm in this case).

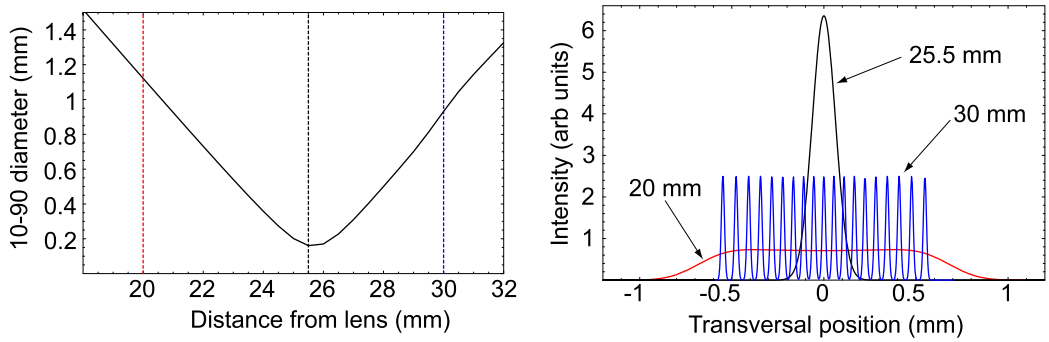

Figure 4.17 Left: Calculated 10-90 beam diameter after a 25 mm lens placed 150 mm behind the BS. Right: Calculated beam profiles at three different positions indicated by the dashed lines in the left graph

By studying equation (4.12) we see that the size of the focused spot is inversely proportional with the focused beam radius at the BS. In Figure 4.18 the calculated shape of the focused beam after a 25 mm lens is shown for two different beam waists at the BS. We see that to obtain a minimum pump mode volume in the laser rod, the beam waist at the BS should be chosen as large as possible while still maintaining good transmission through the BS.

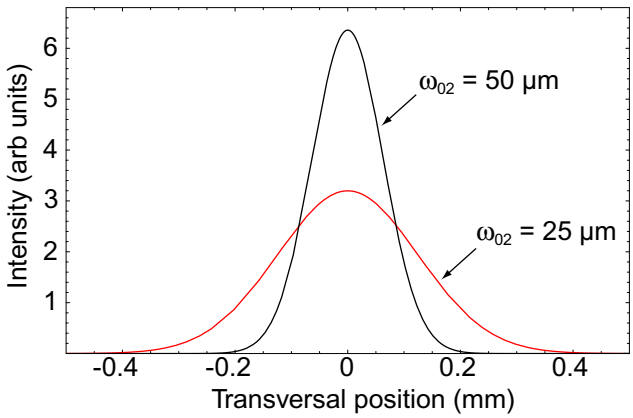

Figure 4.18 Calculated shape of a beam (in the y-direction) in the focal plane after a 25 mm lens placed 150 mm behind the BS

[1] The 10-90 diameter is defined as the distance between the positions (x_0) where the normalized (knife-edge) integral $\int_{-\infty}^{x_0} f(x)dx \Big/ \int_{-\infty}^{\infty} f(x)dx$ equals 0.1 and 0.9

4.1.5 Beam symmetry in the laser rod

When using the focused beam to end-pump a laser rod one would prefer the beam to be circularly symmetric over the pump absorption length in the laser rod. From the discussion made above it is clear that this cannot generally be achieved. If the absorption length was sufficiently short, the beam divergence would not be of any importance, so in that case w_x and w_y could easily be made equal and with a good matching to the TEM_{00} mode of the laser resonator. However, relevant laser materials have absorption lengths of several mm, and over this length the asymmetry will be substantial. In Figure 4.19, the calculated beam diameter in the x- and y-directions are shown as function of distance from the common focus inside YAG (refractive index = 1.82). To obtain the common focus, the f_4 = 50 mm lens in the x-direction was placed 150 mm from the BS and the f_5 = 40 mm lens in the y-direction was placed 35 mm behind L4. In the x-direction, the diameter is found where the intensity is $1/e^2$ of its peak value, while in y-direction the $1/e^2$ diameter is found by multiplying the 10-90 diameter found from knife-edge integration over the beam profile by 1.56 (i.e. assuming a Gaussian cross-section).

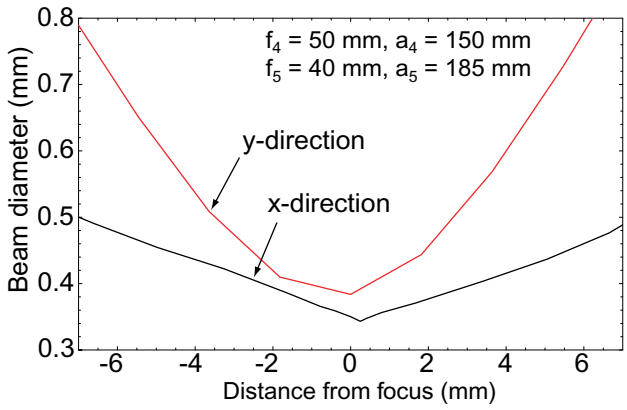

Figure 4.19 Approximate $1/e^2$ beam diameters in a YAG laser rod after focusing the pump beam with 50/40 mm cylindrical lenses in the x-/y-direction placed 150/185 mm behind the BS

The asymmetry shown in Figure 4.19 will have two detrimental effects on the pumped laser: First, the difference in gain region in the two directions may lead to a multi-transverse mode in one or both directions, and, secondly, the difference in thermal lens may lead to different resonator stability conditions in the two directions. The optimal focusing in the two directions will depend on the absorption length, resonator mode size, resonator losses, gain, and thermal lensing effects (the 2 latter effects being dependent on the pump power).

Another possibility is to launch the focused beam into an optical fiber. The beam leaving the fiber will then be circularly symmetric and can be refocused to yield a symmetric pump beam in the laser rod. The main disadvantages of that method are the need for additional optical components, a depolarized pump beam, a certain pump power loss, and a slightly poorer overall beam quality.

4.2 Alignment of the beam shaper

4.2.1 The lenses before the beam shaper

The distances listed in this section are for the special case studied in this work, with cylindrical lenses from Melles Griot: L1: f = 25.4 mm, product #: 01LCP006, L2: f = 60 mm, product # 01LCP005, and L3: f = 50 mm, product # 01LCP133.

The distance from the laser diode to the BS should be 14-15 cm (14.5 cm to the exit aperture). Start by placing lenses L1-3 in their approximate positions. The use of an alignment beam may help ensure that the lenses are at the correct x- and y-positions and that they (L2 and L3) are perpendicular to the beam. The tilt of L1 (to reduce the smile effect, see Figure 4.11) can be adjusted by monitoring the reflected alignment beam. The beam from the laser diode should be monitored with an IR-card or by a camera. A suggested procedure to obtain the correct z-positions of the lenses is as follows: Position L2 such that the beam waist in the y-direction is placed at the center of the BS. As could be seen from (4.7), the position of this waist is close to the focal plane of L2. However, an error in this position of a few mm has only negligible effect on the transmission. Next, L1 should be positioned 25-30 mm from the laser diode (distance to flat back side of lens, see Figure 4.6 and Figure 4.10), and L3 should be adjusted to collimate the pump beam. The distance between the plane surfaces of the two lenses should be approximately 66 mm.

4.2.2 The beam shaper

If the beam shaper consists of two independently adjustable mirrors, a proper alignment procedure could be as follows:
Start with the mirror the beam first 'hits' (the mirror to the right in Figure 4.1). θ and ϕ can easily be aligned by monitoring the reflection of the laser diode on the optical table. The position of this point is:

$$\begin{aligned} x_{Hit} &= h\frac{\sin\phi}{\tan\theta} \\ z_{Hit} &= h\left(\frac{1}{2\sin 2\theta\cos\phi} - \frac{\cos\phi}{\tan\theta}\right) \end{aligned}, \tag{4.15}$$

where h is the height of the beam above the optical board and the position is relative to the point of reflection at the beam shaper mirror. After this alignment, the angle γ needs to be adjusted, for instance by comparison with a vertical reference looking in the opposite direction of the laser beam (with the laser beam turned off). In the x-direction, the mirror should be placed to reflect all but the outmost emitter. When this procedure is done, the mirror closest to the laser can be inserted. The top edge should be horizontal and placed in height close to the beam, but underneath it. This mirror is parallel with the first mirror when the transmitted beams are propagating in parallel in the z-direction. The distance between the mirrors and the height of the mirror closest to the laser should then be adjusted assuring a one-to-one emitter stacking at the exit aperture and to assure optimum transmission.

4.2.3 Alignment tolerances

4.2.3.1 Mirror height

The tolerance for the height adjustment of the mirror closest to the laser is approximately ±20 µm, as can be seen in Figure 4.20 where the input aperture transmission is plotted as function of mirror height. In these simulations, ω_{02} = 50 µm and Δ_y = 300 µm were assumed.

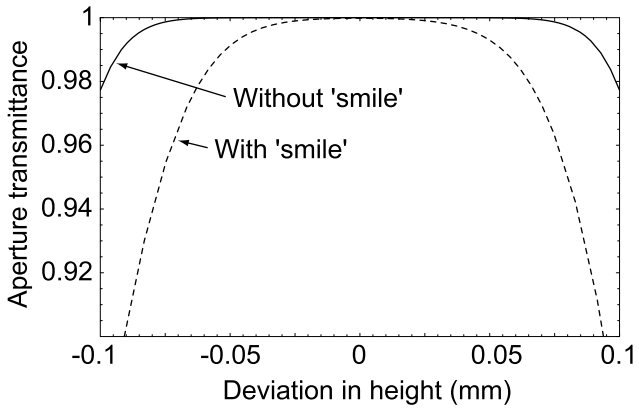

Figure 4.20 Calculated transmission through the input aperture of the BS as function of height of the mirror closest to the diode. A compensated smile-effect is accounted for, ω_{02} is 50 µm, and the input aperture is 300 µm

4.2.3.2 Mirror parallelism

If the mirrors fail to be parallel by an angle δ, each sub-beam will be 2δ off angle with the adjacent sub-beam, and the angle between the top and bottom beams will be 36δ. A misalignment of 0.2 mrad, which is caused by a 10 µm error in mirror spacing across a 50 mm wide mirror, will thus lead to an angle difference of 7.2 mrad between the top and bottom sub-beams. If this error was entirely in the x-direction, this will cause a deviation from a vertical line (top to bottom sub-beam) of ~1 mm at L4 150 mm behind the BS, leading to a larger focus and a poorer beam quality (see below). If this error was entirely in the y-direction, the effect will depend on whether the total beam is diverging or converging. A diverging beam will, in fact, lead to a smaller focus because the focus becomes closer to the waists of the sub-beams (see Figure 4.17). For comparison, the deviation from perfect collimation in the x-direction owing to aberrations in the lens system before the BS is less than 5 mrad.

4.2.3.3 Mirror spacing

From (4.1) we find that an error of ±20 µm in mirror spacing results in a 0.5 mm deviation from a vertical line from top to bottom of the stack of sub-beams, assuming a 300 µm input aperture. This will lead to a slight clipping at the exit aperture. Disregarding this clipping, a 0.5 mm deviation from a vertical line at L4 leads to an increase in the size of the focus in the x-direction to ~0.45 mm (from 0.35 mm), and a subsequent increase in BQ_x from 20 mm·mrad to 30 mm·mrad. In these calculations, f_4 = 50 mm and a_4 = 150 mm, as in Figure 4.16.

4.2.3.4 Vertical exit aperture

The perhaps most difficult part of the alignment procedure is to assure that the exit aperture is vertical (adjustment of γ). An error of 80 mrad leads to ~0.5 mm deviation from a vertical line from top to bottom of the stack of sub-beams. The results on the beam quality in the x-direction are the same as above.

4.3 The non-imaging beam shaper

The BS described so far has been based on imaging the diode bar at the position of the BS and stacking the emitters vertically. There are two main advantages by this. First, the light from the diode will be more symmetrical and easier to focus into a laser rod. Second, the brightness may be increased by removing the 'dead space' between the emitters. However, as was discussed in connection with Figure 4.10, it is practically impossible to image diode arrays with $\gtrsim$ 30 emitters (e.g. the diodes from IMC with 48 emitters along the 1 cm bar) in such a way that all are transmitted without clipping through the exit aperture of the BS. In this case there is no increase in brightness through the BS. However, the alignment of the BS can be a lot easier: Failing to image the emitters will remove the requirement that the exit aperture is exactly equal to the emitter distance, thus removing the strict limitation on the distance between the mirrors.

The non-imaging BS can be described by the following functions: The input and exit apertures are given by Δ_y and Δ_x from (4.1), respectively. The height of the output beam from the BS can be approximated by

$$H_{exit} = ceiling\left(\frac{M \cdot w_{diode}}{\Delta_x}\right)\Delta_y \approx M \cdot w_{diode}\frac{\tan(\theta)}{\sin(\phi)}, \tag{4.16}$$

where w_{diode} ($\approx N{\cdot}d$) is the width of the diode bar, and the *ceiling*-function returns the smallest integer equal to or above its argument.

The output from the BS is still focused by two crossed cylindrical lenses into the laser rod. The size of the image in the x-direction is given by

$$w_x = \Delta_x \frac{f_4}{a_4 - f_4}, \tag{4.17}$$

where the symbols were defined in Figure 4.14. The far field divergence angle is given by (4.10). In the y-direction, assuming that the Gaussian nature of the beam is retained, the size of the focus is still given by (4.12), whereas the far field divergence angle in analogy with (4.13) is given as

$$\alpha_y = \frac{H_{exit}}{f_5}. \tag{4.18}$$

The beam qualities are given by

$$BQ_x = w_x\alpha_x = \frac{\Delta_x}{M}\alpha = \frac{\Delta_x}{M \cdot w} BQ_x^I$$
$$BQ_y = w_y\alpha_y = 2\frac{\lambda}{\pi \cdot \omega_{02}} H_{exit} = \frac{H_{exit}}{N \cdot \Delta_y^I} BQ_y^I \quad , \tag{4.19}$$

where $BQ_{x/y}{}^I$ is are the beam qualities in the case of the imaging BS as defined in (4.11) and (4.14), and $\Delta_y{}^I$ is the vertical displacement in the imaging BS. If we calculate the beam quality product, i.e. $BQ = BQ_x \cdot BQ_y$, we find that in the case of equal input apertures, $BQ \approx d/w\ BQ^I$. This stems from that the 'dead space' between the emitters is not removed with the non-imaging geometry. It should be noted that these calculations neglect diffraction at the vertical edge in the exit aperture. Diffraction may somewhat reduce the beam quality.

From (4.19) we see that the ratio of the beam qualities of the non-imaging and imaging BS scales with the ratio of the size of the output beam in each direction. Thus, from (4.19) and (4.16) it is clear that the output beam can be made more symmetric by a proper choice of Δ_x. This is illustrated in Figure 4.21, where the calculated beam qualities are shown as function of Δ_x for the Coherent diode. We observe that the beam qualities become equal for the given parameters when $\Delta_x \approx 1.5$ mm. For a diode bar with higher divergence in the x-direction, BQ_x becomes poorer, and the value of Δ_x for the IMC-diodes where the beam qualities are approximately equal is $\Delta_x \approx 1$ mm.

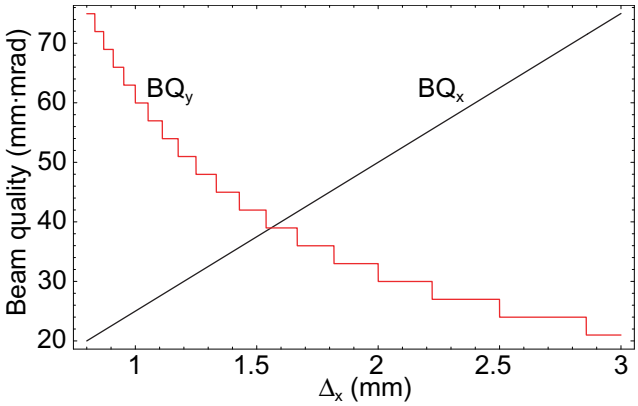

Figure 4.21 *Calculated beam quality in the x- and y-direction after a non-imaging BS as function of the horizontal displacement Δ_x. In the calculations, $w_{diode} = 10$ mm, $\alpha = 50$ mrad, $M = 2$, $\omega_{02}=50$ µm, and $\Delta_y = 0.3$ mm. The stepwise behavior of BQ_y stems from the ceiling-function.*

Since the requirement of imaging is lifted, the lens system between the diode and the BS can be chosen differently than before. The primary requirements are now that the beam is collimated in the x-direction and focused as before in the y-direction. The lens system may also be chosen for an appropriate value of M. The compensation for smile is still desired, but one may choose to increase the input aperture (Δ_y) to reduce the sensitivity to smile at the cost of a poorer beam quality in this direction.

5 RESULTS

In this Section the resulting beam after the BS is characterized for the three different laser diode bars described in Section 3. The results depend to some extent on the actual parameters of the laser diode itself, e g smile-effect and transversal mode pattern, but nevertheless give a good indication of what is possible with the BS technology.

The beam quality was found by measuring how the $1/e^2$ beam radius evolved around the focal plane of a cylindrical lens. This was then fit to a curve calculated for a beam whose divergence was M^2 times that of a fundamental Gaussian beam. For wavelengths ~800 nm, this value is the same as the mm·mrad value. The values are vulnerable to errors in measurements of the smallest diameter and have therefore considerable uncertainty connected to them.

5.1 Imaging beam shaper

The Coherent laser diode bar consisted of 19 emitters, and it was therefore possible to use the imaging BS. The diode delivered 30 W at 32 A driving current. With 350 µm input aperture, 24.5 W was transmitted to the focal plane behind the BS and two crossed cylindrical lenses. The intensity profile of the beam in the focal plane is shown in Figure 5.1. In Figure 5.2, the measured beam size is shown for different distances around the focal plane. The curves indicate the $1/e^2$ value of the peak intensity. We notice the clear similarity between the behavior of the curves in the y-direction and the calculated curves in Figure 4.17. The curves used to find the beam quality are shown in Figure 5.3.

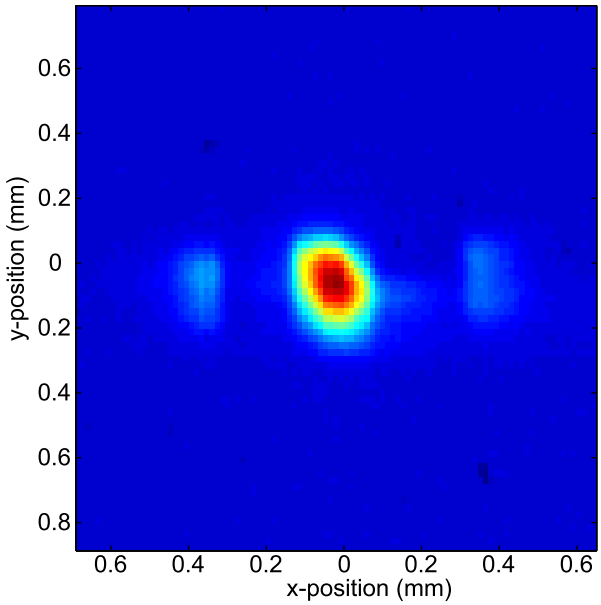

Figure 5.1 Measured intensity profile in the focal plane of two crossed 40 mm cylindrical lenses

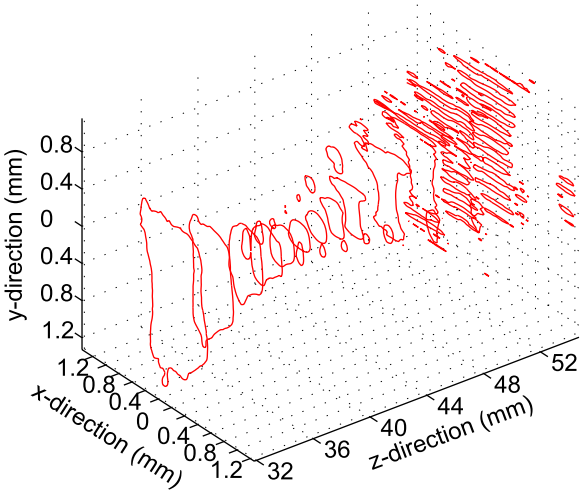

Figure 5.2 *Measured beam profile as function of z-position behind two crossed 40 mm cylindrical lenses*

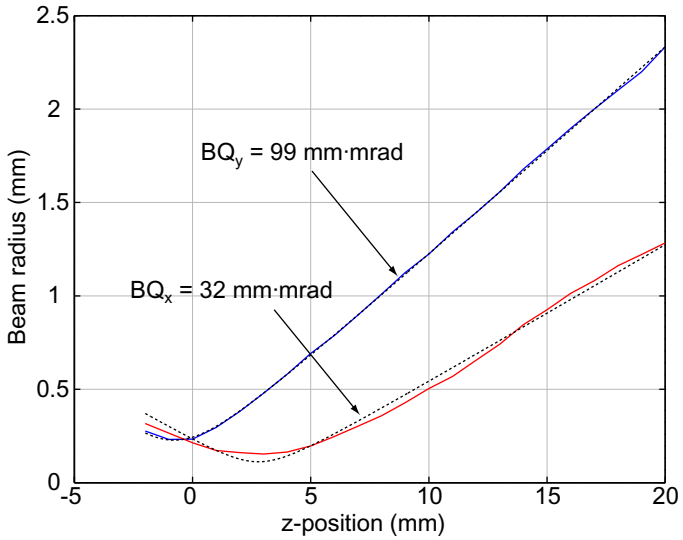

Figure 5.3 *Measured beam radius as function of z-position after two crossed 40 mm cylindrical lenses. The dashed curves are the best fits to Gaussian beams and give the beam quality of the beam*

5.2 Non-imaging beam shaper

The IMC diode bars consist of 48 emitters each, and it is therefore not practically possible to use the imaging BS geometry, both because of the narrower distance between adjacent emitters and because of the larger divergence in the x-direction from each emitter. For practical reasons, the parameters of the non-imaging BS system was approximately the same as for the imaging BS, with a ~300 µm input aperture and ~20 stacked beams in the y-direction at the exit aperture.

5.2.1 IMC diode S/N 3114

With a 300 µm input aperture, 35 W was transmitted through the BS and a pair of crossed cylindrical lenses at a driving current of 52.5 A. The output from the laser diode was 46 W at this driving current. In Figure 5.4, the measured beam profile in the focal plane behind two crossed cylindrical lenses is shown (f_x = 50 mm and f_y = 60 mm). We observe that the beam

diameter is approximately 0.5 mm in both directions. The z-dependence of the beam size is shown in Figure 5.5. We note that the beam appears to be reasonably symmetric over a distance of ~10 mm. The beam quality was found to be ~ 70 mm·mrad in the x-direction and ~ 103 mm·mrad in the y-direction, as is shown in Figure 5.6.

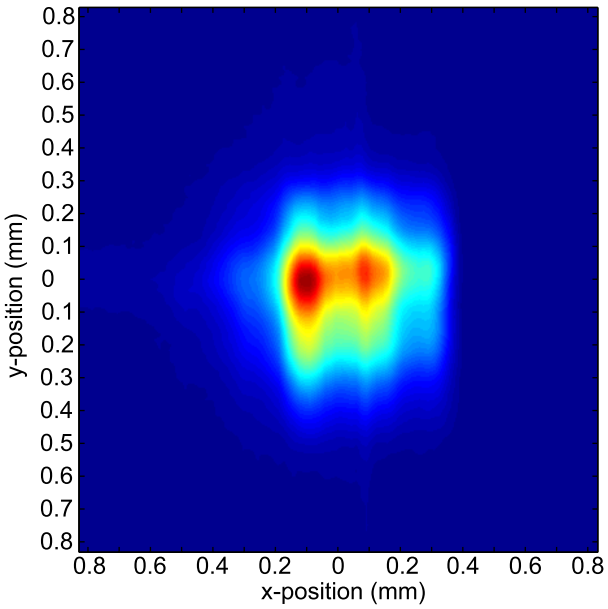

Figure 5.4 *Measured beam profile in the focal plane of two crossed cylindrical lenses (f_x = 50 mm and f_y = 60 mm)*

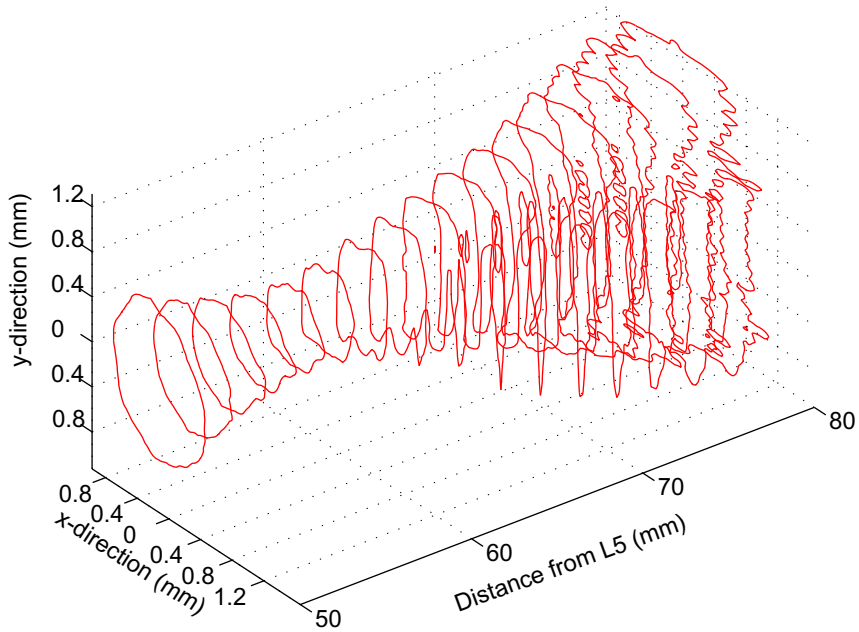

Figure 5.5 *Measured beam profile as function of z-position behind two crossed cylindrical lenses, f_x = 50 mm and f_y = 60 mm*

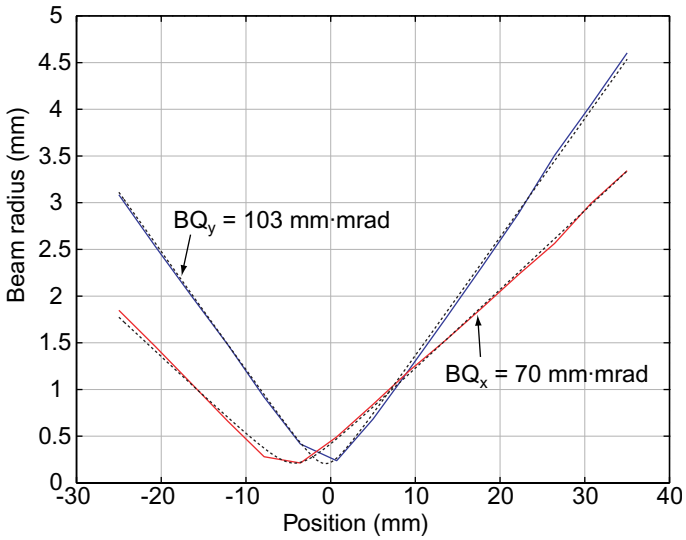

Figure 5.6 *Measured beam radius as function of z-position after two crossed cylindrical lenses, f_x = 50 mm and f_y = 60 mm. The dashed curves are the best fits to Gaussian beams and give the beam quality of the beam*

5.2.2 IMC diode S/N 3180

In Figure 5.7, the measured beam profile in the focal plane behind two crossed cylindrical lenses is shown (f_x = 50 mm and f_y = 60 mm). We observe that the beam diameter is somewhat larger than for the other IMC diode; approximately 0.6 mm in the y-direction and 0.8 mm in the x-direction. The z-dependence of the beam size is shown in Figure 5.8 and Figure 5.9. We note that the beam is reasonably symmetric over a distance of ~10 mm in air. The beam quality was found to be ~ 77 mm·mrad in the x-direction and ~ 107 mm·mrad in the y-direction, as is shown in Figure 5.9. Of the 46 W output power from the laser diode at 52.5 A driving current, 34.2 W was available at the focal plane of lens 4 and 5 with 380 µm input aperture of the BS.

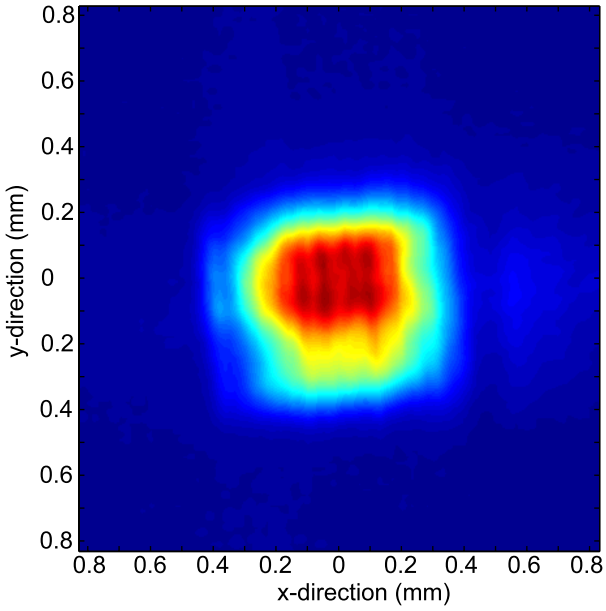

Figure 5.7 *Measured beam profile in the focal plane of two crossed cylindrical lenses, f_x = 50 mm and f_y = 60 mm*

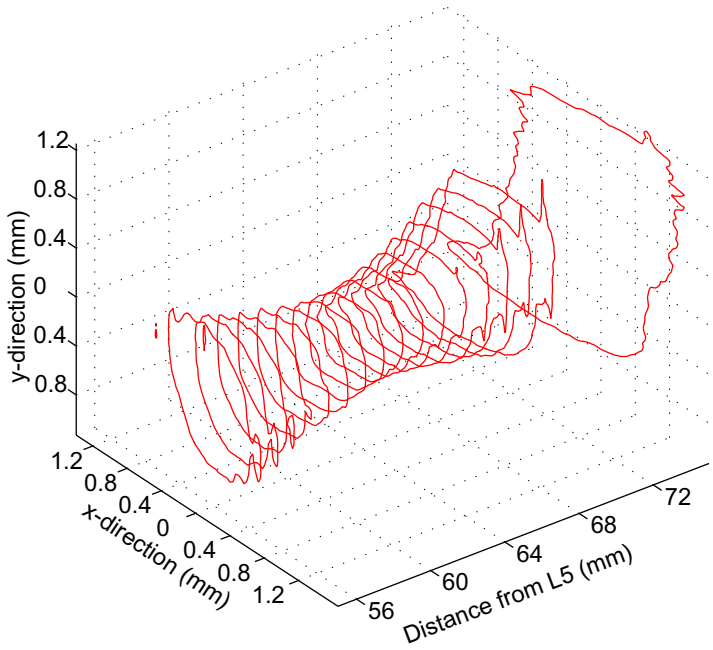

Figure 5.8 *Measured beam profile as function of z-position behind two crossed cylindrical lenses, f_x = 50 mm and f_y = 60 mm. The curves correspond to $1/e^2$ of the peak value*

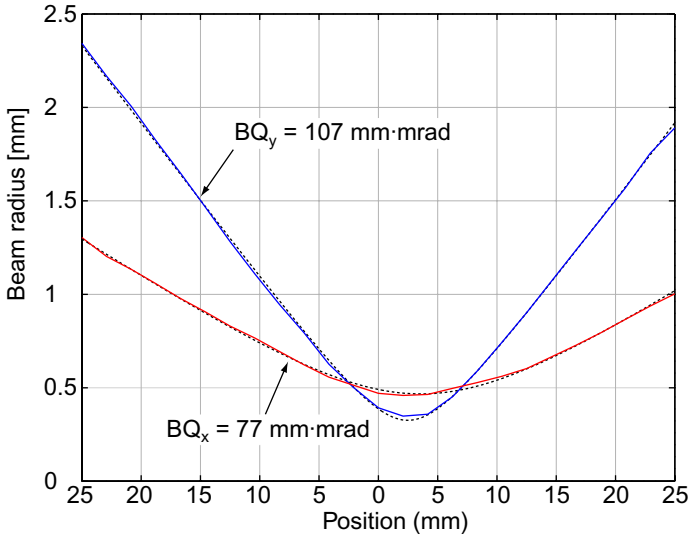

Figure 5.9 *Measured beam radius as function of z-position after two crossed cylindrical lenses (f_x = 50 mm and f_y = 60 mm). The dashed curves are the best fits to Gaussian beams and give the beam quality of the beam*

5.3 Summary of results

The results for the three laser diode bars are summarized in Table 3.1. As expected, the beam quality of the imaging geometry is better than that from the non-imaging geometry, in particular in the x-direction. For all cases, however, the measured beam qualities are about 50% poorer than the calculated ones (from calculations and simulations previously in this work). Some of this discrepancy can be ascribed to the uncertainty in finding the smallest beam radius in the measurements. Also, the beam radius may not be well-defined for a non-Gaussian beam profile. Further, the assumed beam quality from the laser diode may be incorrect, for example will α = 70 mrad instead of 50 mrad increase the calculated BQ_x from 20

to 32 mm·mrad for the Coherent diode. In the y-direction, the smile-effect has a detrimental effect on the beam quality, but was not accounted for in the calculations. Uncertainty in the values of ω_{02}, Δ_x and Δ_y also influence on the calculated beam quality according to Equations (4.14) and (4.19). Additionally, it was observed after the measurements that the exit aperture of IMC3180 was slightly non-vertical.

	Geom.	Δ_x	Δ_y	P_{diode}	P_{trans}	f_4	f_5	a_4	w_x	w_y	Measured		Calculated	
		mm	mm	W	W	mm	mm	mm	mm	mm	BQ_x	BQ_y	BQ_x	BQ_y
Coherent	I	1.0	0.35	30	24.5	40	40	150	0.45	0.35	32	99	20	67
IMC3114	N-I	0.8	0.30	46	35.2	40	40	170	0.5	0.5	70	103	48	72
IMC3180	N-I	1.0	0.38	46	34.2	50	60	147	0.9	0.7	77	107	59	76

Table 5.1 Summary of results from beam shaping of laser diode bars. Units for BQ are in mm·mrad

6 CONCLUSIONS

Beam shaping of the output from laser diode bars is a powerful technique for efficient coupling of pump light into high-power end-pumped solid-state lasers. Using the parallel mirrors technique originally developed at the University of Southampton, we have demonstrated beam shaping of the highly astigmatic output from 1 cm wide diode bars, and focused the resulting beam to less than 0.5 mm diameter spot with reasonably good symmetry over a 10 mm distance around the focal plane.

By a thorough theoretical approach to the beam shaper system, we have identified two operating regimes: The imaging and the non-imaging beam shaper. In the imaging beam shaper, each emitter of the laser diode bar is imaged by a set of cylindrical lenses onto the mirrors of the beam shaper, where the sub-beams can be stacked and rearranged. In the non-imaging beam shaper, the light from the laser diode bar is still transferred to the mirrors of the beam shaper, but the requirement of imaging the emitters is lifted. This will normally result in a somewhat poorer beam quality, but also in greater flexibility in design and alignment of the system. The size of the emitters, the distance between the emitters, and the divergence from the emitters determine whether the imaging regime can be used or not. There are in general two different geometries of high-power laser diode bars. One type consists of ~20 emitters with ~30% fill-factor of the 1 cm diode bar. This can be used with the imaging beam shaper. The other type consists of ~50 emitters with ~50% fill-factor. This should be used with the non-imaging beam shaper.

There are other parameters of the laser diode bar that have impact on the transmission through the beam shaper system. These are the smile-effect of the laser diode, i.e. the diode bar's deviation from a straight line in the x-direction, and the transversal mode pattern in the y-direction. The latter has often been considered to be that of the fundamental Gaussian, but our measurements have shown that this is not the case. Both these effects have been seen to vary considerably from diode to diode.

In Figure 6.1 a photograph of the experimental realization of a laser-diode with a beam shaping system is shown. The small footprint (~10 cm x 20 cm) makes this a flexible and attractive building block for high-power diode-end-pumped solid-state lasers.

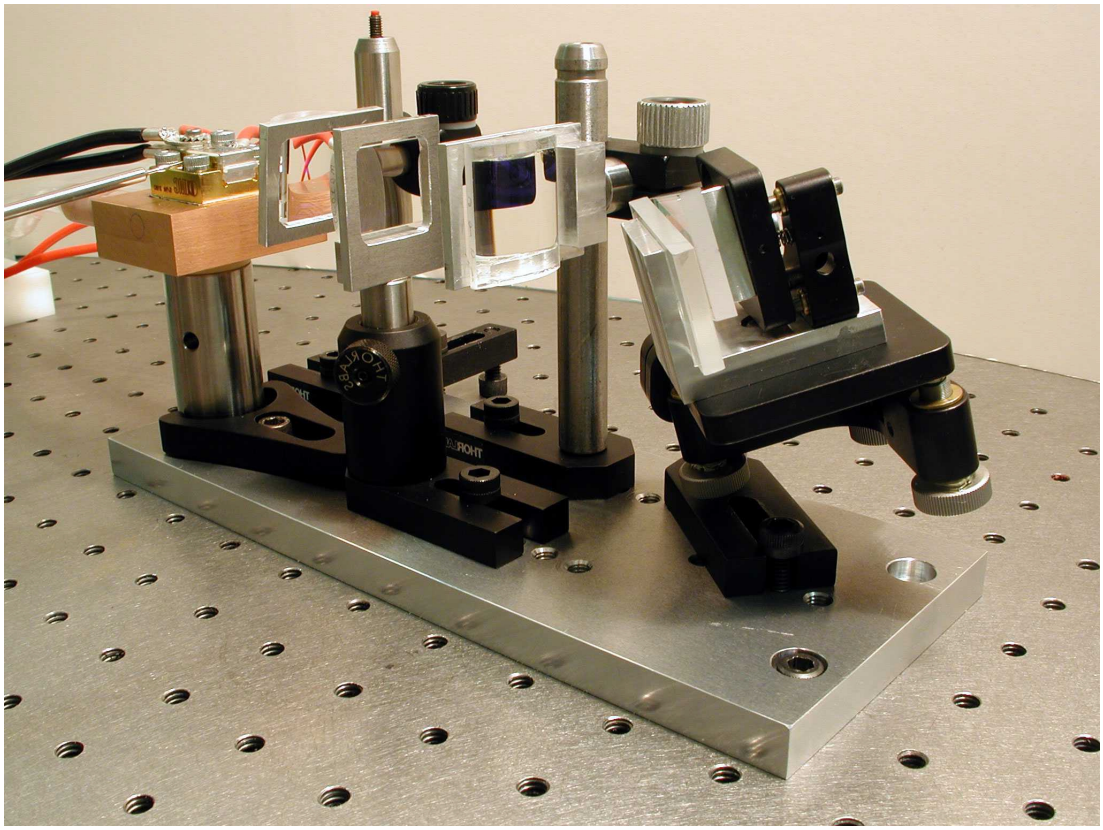

Figure 6.1 Photograph of a laser diode with optics and beam shaper

References

[1] G Rustad. *Diodelaser endepumpet Tm:YAG laser*. FFI/Rapport-98/02171, Norwegian Defence Research Establishment, Kjeller, 1998.

[2] G Rustad and K Stenersen. Low threshold laser-diode side-pumped Tm:YAG and Tm:Ho:YAG lasers. *IEEE J. Sel. Top. Quantum Electron.*, 3: 82-89, 1997.

[3] G Rustad. *Modelling and experimental investigation of laser-diode end-pumped and side-pumped thulium- and holmium doped lasers*. FFI/Rapport-95/01238, Norwegian Defence Research Establishment, Kjeller, 1995.

[4] W A Clarkson and D C Hanna. Two-mirror beam-shaping technique for high-power diode bars. *Opt. Lett.*, 21: 375-377, 1996.

[5] T Graf and J E Balmer. High-power Nd:YLF laser end pumped by a diode-laser bar. *Opt. Lett.*, 18: 1317-1319, 1993.

[6] H Zbinden and J E Balmer. Q-switched Nd:YLF laser end pumped by a diode-laser bar. *Opt. Lett.*, 15: 1014-1016, 1990.

[7] S Yamaguchi, T Kobayashi, Y Saito, and K Chiba. Collimation of emissions fra a high-power multistripe laser-diode bar with multiprism array coupling and focusing to a small spot. *Opt. Lett.*, 20: 898-900, 1995.

[8] S Yamaguchi, T Kobayashi, Y Saito, and K Chiba. Collimation of emission from a 1-cm aperture tightly arranged, multistripe laser-diode bar with a multiprism array coupling. *Appl. Opt.*, 39: 1875-1878, 1997.

[9] K Du, Y Liao, and P Loosen. Nd:YAG slab laser end-pumped by laser-diode stacks and its beam shaping. *Opt. Commun.*, 140: 53-56, 1997.

[10] J R Leger and W C Goltsos. Geometrical transformation of linear diode-laser arrays for longitudinal pumping of solid-state lasers. *IEEE J. Quantum Electron.*, 28: 1088-1100, 1992.

[11] T S Rose, J S Swenson, and R A Fields. High-efficiency longitudinal diode-bar pumping of solid-state lasers. In: *Diode pumping of average-power solid state lasers*, Proc. SPIE vol 1865, G F Albrecht, R J Beach, and S P Velsko, eds (SPIE, Bellingham, WA, 1993), pp 56-60.

[12] S Yamaguchi and H Imai. Efficient Nd:YAG laser end-pumped by a 1 cm aperture laser-diode bar with a GRIN lens array coupling. *IEEE J. Quantum Electron.*, 28: 1101-1105, 1992.

[13] C P Wyss, W Lüthy, H P Weber, L Brovelli, C Harder, and H P Meier. A diode-laser pump source with small focus diameter for end-pumped systems. *Opt. Quantum Electron.*, 31: 173-181, 1999.

[14] R J Beach, P Reichert, W Benett, B Freitas, S Mitchell, A Velsko, J Davin, and R Solarz. Scalable diode-end-pumping technology applied to a 100-mJ Q-switched Nd^{3+}:YLF laser oscillator. *Opt. Lett.*, 18: 1326-1328, 1993.

DISTRIBUTION LIST

FFIE **Dato:** 15 mai 2001

RAPPORTTYPE (KRYSS AV)	RAPPORT NR.	REFERANSE	RAPPORTENS DATO
X RAPP ☐ NOTAT ☐ RR	2001/02647	FFIE/792/115	15 mai 2001
RAPPORTENS BESKYTTELSESGRAD		ANTALL EKS UTSTEDT	ANTALL SIDER
Unclassified		45	41
RAPPORTENS TITTEL		FORFATTER(E)	
BEAM SHAPING OF HIGH POWER LASER DIODE BARS		RUSTAD Gunnar, LIPPERT Espen, STENERSEN Knut	
FORDELING GODKJENT AV FORSKNINGSSJEF:		FORDELING GODKJENT AV AVDELINGSSJEF:	

EKSTERN FORDELING

ANTALL	EKS NR	TIL
1		FO/FST
1		FO/FST v/Oblt Gaute Dyrdal
1		LTI, EK-kontoret
1		HFK
1		HFK v/Rittm Tarjei Holtestaul
1		HFK v/Overing Jan I Smeland
1		LFK
1		LFK, v/Kapt Egil Strømsvåg
1		SFK
1		SFK, v/Orlkapt Bjarne Isfeldt
		www.ffi.no

INTERN FORDELING

ANTALL	EKS NR	TIL
14		FFI-Bibl
1		Adm direktør/stabssjef
1		FFIE
1		FFISYS
1		FFIBM
1		FFIN
1		Halvor Ajer, FFIE
1		Gunnar Arisholm, FFIE
1		Trond Brudevoll, FFIE
1		Harald Hovland, FFIE
1		Espen Lippert, FFIE
1		Stian Løvold, FFIE
2		Gunnar Rustad, FFIE
1		Knut Stenersen, FFIE
1		Asta S Villanger, FFIE
1		Gunnar Wang, FFIE
5		Arkiv, FFIE
		FFI-veven

FFI-K1 Retningslinjer for fordeling og forsendelse er gitt i Oraklet, Bind I, Bestemmelser om publikasjoner for Forsvarets forskningsinstitutt, pkt 2 og 5. Benytt ny side om nødvendig.